The genomics and physiology of abiotic stressors associated with global elevation gradients in *Arabidopsis thaliana*

Short Title: Global elevational clines in Arabidopsis

Diana Gamba[1,*], Claire Lorts[1], Asnake Haile[1,2], Seema Sahay[3], Lua Lopez[1,4], Tian Xia[1], Evelyn Kulesza[1,5], Dinakaran Elango[5,6], Jeffrey Kerby[7], Mistire Yifru[2], Collins E. Bulafu[8], Tigist Wondimu[2], Katarzyna Glowacka[3], Jesse R. Lasky[1]

[1]Department of Biology,
Pennsylvania State University,
University Park, PA 16802, USA

[2]Department of Plant Biology and Biodiversity Management,
Addis Ababa University,
Addis Ababa, Ethiopia

[3]Department of Biochemistry,
University of Nebraska-Lincoln,
Lincoln, NE 68588, USA

[4]Department of Biology,
California State University San Bernardino,
San Bernardino, CA 92407, USA

[5]Department of Plant Science,
Pennsylvania State University,
University Park, PA 16802, USA

[6]Department of Agronomy,
Iowa State University,
Ames, IA 50011, USA

[7]Aarhus Institute for Advanced Studies,
1630, Høegh-Guldbergs Gade 6B,
Aarhus, Denmark 8000

[8]Department of Plant Sciences, Microbiology, and Biotechnology,
Makarere University,
Kampala, Uganda

*Corresponding Author
dxg5484@psu.edu

Abstract

Arabidopsis thaliana has a wide elevational range and much of its diversity may be associated with local adaptation to elevation. We took a multi-regional view of the genomics and physiology of elevational adaptation in Arabidopsis, with >200 ecotypes, including 17 newly collected from Africa. We measured plant responses to potential high elevation stressors: low pCO_2, high light, and night freezing and conducted genome-wide association studies (GWAS). We found evidence of an adaptive cline in the western Mediterranean with low $\delta^{13}C$/early flowering at low elevations to high $\delta^{13}C$/late flowering at high elevations. By contrast, central Asian high elevation ecotypes flowered earlier. Antioxidants and pigmentation under high light and freezing showed regional differentiation but not elevational clines and may be associated with maladaptive plasticity. We found natural variation in non-photochemical quenching (NPQ) kinetics in response to chilling and fluctuating light, though with an unclear role in local adaptation. There were several candidate genetic loci mapped, including the ascorbate transporter PHT4;4 (associated with antioxidants) that influences the xanthophyll cycle, and may be involved in local adaptation to Morocco. Our study shows how the ecological strategies and genetic loci causing local adaptation to elevation change across regions and contribute to diversity in Arabidopsis.

Introduction

Changes in environmental conditions with changing elevation are some of the most iconic natural gradients (Caldas, 1966). Correspondingly, changes in plant growth forms are dramatic over hundreds or thousands of meters of elevation (Caldas, 1966; Hedberg, 1964; Körner, 2021). Elevational gradients also are a key factor driving local adaptation, and hence diversity, within species that have broad elevational ranges (Clausen et al., 1940; Kooyers et al., 2015). At high elevations in particular, the combination of cold and high light during vegetative periods poses a major challenge. Additional environmental changes from sea level to alpine environments include decreased average temperature, wider fluctuations in daily temperature, altered (i.e., orographic) precipitation and cloud patterns, and shorter growing seasons (Körner, 2003, 2007). While local adaptation to specific environmental conditions has often been observed in reciprocal transplants and common gardens (Clausen et al., 1940; Anderson et al., 2014; Ågren and Schemske, 2012; Fournier-Level et al., 2011; Ward and Strain, 1997), the physiology and genetic basis of local adaptation to high elevation sites is often less clear.

Photosynthesis is at the nexus of multiple physiological challenges for high elevation plants. First, partial CO_2 declines approximately linearly with elevation, for example at 4000 m being only ~65% of sea level pCO_2 (Körner, 2021). Species from high elevations may exhibit higher fitness and better regulation of physiological processes under low atmospheric pCO_2 atmospheric (Ward and Strain, 1997; Zhu et al., 2010). However, CO_2 limitation is likely counteracted by elevational reductions in pO_2 and photorespiration (Wang et al., 2017). Second, clear sky radiation increases with elevation, but cold temperatures slow the dark reactions of photosynthesis, leading to potential photo-oxidative damage if oxidizing photons are not properly handled (Wise, 1995). Third, alpine environments can experience extreme temperature fluctuations, often reaching below freezing temperatures every night, which not only exacerbates oxidative damage but can also physically damage cells (Suzuki and Mittler, 2006). Finally, while temperature more consistently decreases with elevation, different regions may show different elevational clines in cloudiness, resulting in fluctuating light intensity that complicates elevational light patterns in different geographic regions (Körner, 2021).

Photo-oxidative damage at low temperatures can be counteracted via several mechanisms. One is non-photochemical chlorophyll fluorescence quenching (NPQ) in which excess absorbed photons dissipate into heat or by the xanthophyll cycle (Muller et al., 2001; García-Plazaola et al., 2012). When light intensity rapidly increases (e.g., due to clearing cloud cover at high elevations), rapid acclimation of NPQ (fast NPQ kinetics) may be adaptive (Rungrat et al., 2019). Another mechanism is the increased production of antioxidant compounds including carotenoids or flavonoids, which can scavenge reactive-oxygen-species (ROS) (Wise, 1995; Schulz et al., 2016; Juszczak et al., 2016; Havaux et al., 2007; Hetherington et al., 1989; Hannah et al., 2006; Li et al., 2017). A remaining goal is to dissect natural variation in these traits and test the role of this variation in local adaptation to high elevations.

One challenge in deriving general conclusions about adaptive responses to elevation for widespread species is that elevational changes in environment often differ from region to region, potentially leading to region-specific local adaptations. Even when gradients are consistent, local adaptation to isolated mountain ranges can occur via shared or distinct genetic and phenotypic mechanisms (Bohutínská et al., 2021). Furthermore, plant adaptation to extreme conditions often comprises complex multivariate responses where homeostatic regulation during photosynthesis is achieved combined with changes in phenology (Smith and Knapp, 1990; Kooyers et al., 2015; Fernández-Marín et al., 2020).

The model plant *Arabidopsis thaliana* (hereafter Arabidopsis) has a broad geographic and elevational range, from below sea level to ~4400 m in Eurasia and Africa, making it an ideal system for studying multi-regional adaptation across elevations (Wolfe and Tonsor, 2014; Luo et al., 2015a; Vasseur et al., 2018). For example, in the Pyrenees low elevation/coastal sites experience summer drought, potentially selecting for higher germination rates and earlier flowering than in high elevation sites (Montesinos-Navarro et al., 2011; Montesinos-Navarro et al., 2012; Picó, 2012; Wolfe and Tonsor, 2014; Vidigal et al., 2016). In the Alps, phenology may also vary with elevation (Suter et al., 2014), but physiological clines are unclear (Luo et al., 2015b; Günther et al., 2016; Lampei et al., 2019). In the western Himalayas flowering time can be plastic in response to temperature, especially in ecotypes from high elevation (Singh and Roy, 2017). Little is known about elevational clines in African Arabidopsis. Arabidopsis habitat in the Atlas Mountains in Morocco is similar climatically to Iberian mountains, but populations in Morocco and sub-Saharan Africa are older than most Eurasians with higher genetic diversity (Brennan et al., 2014; Durvasula et al., 2017; Fulgione and Hancock, 2018). Eastern African populations are among the highest recorded elevations (up to ~4400 m) and though these represent unique environments for Arabidopsis (Brochmann et al., 2021) there have been no phenotypic studies.

Here, we took a multi-regional view of Arabidopsis genomes, life history, and physiology across elevational gradients. We conducted three growth chamber experiments that simulated potential high elevational stressors (Experiment 1: low pCO_2, Experiment 2: high vs. low light in cool temperatures, and Experiment 3: night-time freezing vs. cool temperatures in high light) using a diverse set of naturally inbred lines (ecotypes). We measured morphological, resource use, life history, photosynthetic, and oxidative-stress related traits. We characterized climatic gradients and tested for adaptive elevational clines in four geographic regions: the western Mediterranean, Europe, central Asia, and eastern Africa (including previously unstudied populations). We performed genome-wide association studies (GWAS) to map loci causing trait variation and tested if selection maintains trait variation. We tested the following hypotheses:

1. Under low pCO_2, ecotypes from higher elevations would be more efficient in conserving resources, which could in turn be related with a conservative life history strategy of lower photosynthetic rates and a late flowering life cycle. Alternatively, higher photosynthetic rates and earlier flowering at higher elevations could be advantageous in regions with early/unpredictable summer stress.
2. Antioxidant activity and pigmentation should be higher under high light and night-time freezing and associated with higher fitness in higher elevation ecotypes. The opposite pattern could arise if antioxidants and pigmentation are stress symptoms, i.e., maladaptive plasticity, and high elevation ecotypes are adjusting to those conditions via other mechanisms.
3. Photosynthetic rate is greater and NPQ kinetics are more rapid in ecotypes from higher elevations because light intensity is higher than at low elevations. Alternatively, NPQ kinetics in high elevation ecotypes might be slower and more conservative to minimize oxidative damage.
4. The genetic basis of natural variation in life history and physiology associated with elevational stressors will involve mutations in flowering time and seed dormancy pathways, oxidative stress, antioxidant biosynthetic and transport pathways, and cold tolerance pathways. Trait-associated SNPs will show elevational clines due to local adaptation.

Results

Regional patterns in climate and population genetic structure

To investigate natural phenotypic and genetic variation across elevational gradients in different mountains, we studied a total of 270 Arabidopsis ecotypes, including 261 from native regions, 17 of which were newly collected in eastern Africa (Fig. 1 A, Table S1). Pairwise genetic distances from 205,667 SNPs from whole genome resequencing, filtered for LD and including eight newly sequenced ecotypes from alpine eastern Africa (total N=261), showed that population genetic structure largely corresponded to geographic regions and not elevation. Ecotypes from low and high elevations on the same mountain range were more closely related than ecotypes of similar elevations on different mountains (Fig. 1 B). The Caucasus was an exception, where ecotypes from elevations <1000 m were more closely related to eastern Mediterranean ecotypes but distantly related to nearby but upslope Caucasus ecotypes (>1000 m). These high elevation Caucasus ecotypes were more closely related to central Asian ecotypes, probably due to distinct colonization routes following glacial retreat.

Our regional subsets of ecotypes had different elevational ranges. Central Asia (in our study also including Lebanon, the Caucasus, and the Urals) was largest (-28–3571 m), Europe (4–2560 m) and western Mediterranean (115–2528 m) were similar, while the eastern African range included the highest elevations (2775–4374 m) (Fig. 1). A PCA of 85 climatic variables from the native range of 258 ecotypes with accurate provenance data showed distinct climates occupied by ecotypes in different regions (Fig. 1 C, Table S2), despite substantial elevational variation within regions. We also found strong climatic elevational gradients in each region (Fig. 1 D-G). In general, elevational gradients were similar between regions, with lower minimum/night temperatures at higher elevations. However, while in central Asia, Europe, and the western Mediterranean the length of the growing season decreases with elevation, in eastern Africa it is the opposite, and dry seasons are milder at higher elevations. In contrast, in central Asia and the western Mediterranean drought during the growing season slightly increases with elevation, while in Europe it decreases. In eastern Africa, the ratio of daily to annual temperature variation (isothermality) is high and mostly constant across elevation, while elsewhere isothermality increases at higher elevations.

Figure 1. Provenance, genetic relationships, and climates of studied ecotypes. Ecotypes are colored by region in all plots (central Asia: red, Europe: green, eastern Africa: blue, western Mediterranean: purple), and symbols represent elevation below (circles) and above (triangles) 1000 m for all regions, except for eastern Africa where the threshold is 4000 m. **A**. Geographic location of ecotypes studied. **B**. Neighbor-joining tree based on 261 ecotypes and 205,667 resequencing SNPs filtered for LD. Tips with no symbol are ecotypes outside of the native range. **C**. First and second principal components (PCs) of climate space representing conditions in 258 ecotypes based on 85 climatic variables. Arrows and text summarize loadings more strongly correlated with PC1 and PC2, indicating the direction of the relationship (not proportional to eigenvectors; PET = potential evapotranspiration). **D-G**. Linear regressions of four climatic variables on elevation of origin. Selected variables describe the growing season and isothermality (i.e., the ratio of diurnal to annual variation in temperature). Significant relationships ($p < 0.05$) are depicted with their corresponding adjusted-R^2.

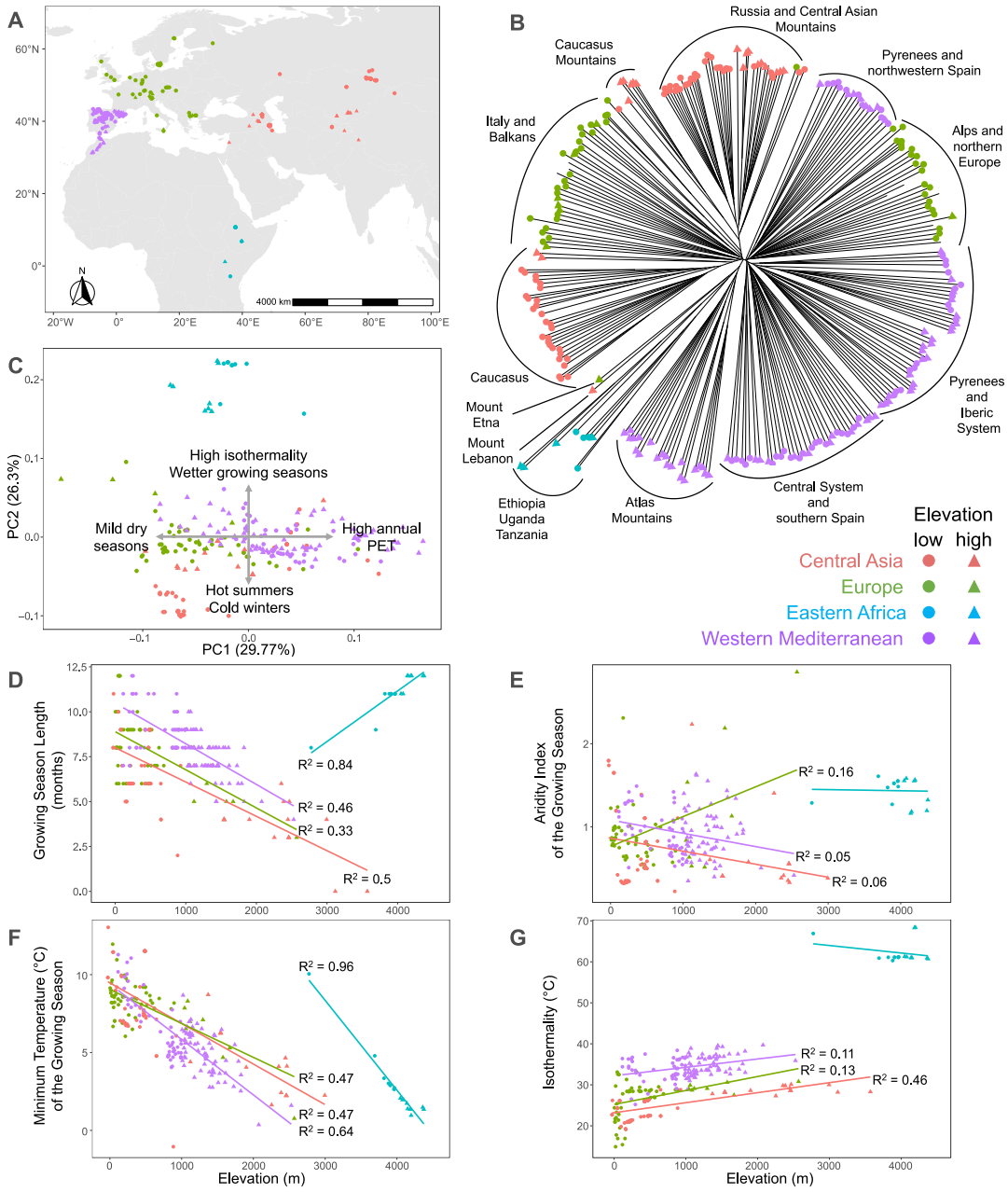

Regional patterns in life history and physiology

To characterize coordinated life history-physiology axes in our ecotypes, we summarized traits in Experiment 1 (cool conditions, moderate moisture, and low pCO_2, Table S3) and flowering time with a Principal Component Analysis (N=215, Fig. S1 A). This PCA shows an association between later flowering, more compact rosettes, and higher $\delta^{13}C$. Despite differences in environment and elevational ranges among regions, there was no clear separation of ecotypes by region or elevation in $PC1_{Exp1}$ and $PC2_{Exp1}$. We also performed pairwise correlations of traits globally and within regions (Fig. S2–S6, Supplemental Results 1), and examined if these traits differed between regions (Supplemental Results 2).

Trait responses to high light and night-time freezing treatments and associations with performance

To characterize genetic variation in physiology and performance under high-elevation associated stressors, our next two experiments imposed contrasting light levels on 111–114 ecotypes (Experiment 2, Table S4) and contrasting night temperatures on 170–172 ecotypes (Experiment 3, Table S5). We measured fresh aboveground mass, total antioxidant activity, and the multidimensional color variation of leaves (Experiment 2) and their extracts (Experiment 3) among genotypes and environments. We evaluated color because pigments can be adaptive as they act as antioxidants under high light and/or cold. We calculated PCA with RGB color values and used the first two principal components in each experiment as our color traits (Fig. S1 B, C, Supplemental Results 3).

In Experiment 2, ecotypes under high light had lower fresh mass ($F(1,214)=51.66$, $p<0.0001$), higher antioxidant activity ($F(1,214)=55.09$, $p<0.0001$), with darker leaves (lower values of $PC1_{LeavesColor}$, $F(1,223)=134.2$, $p<0.0001$) and bluer leaves (higher values of $PC2_{LeavesColor}$, $F(1,223)=51.66$, $p<0.0001$) than when grown under low light (both grown simultaneously at ca. 8.5ºC day, 5.5ºC night, Fig. 2, left panels). Survival rates were slightly but significantly lower under high than low light (93 vs 96%, $F(1,214)=5.80$, $p=0.02$). Furthermore, an ANOVA showed significant differences in antioxidant activity at high light among regions ($F(2,105)=5.93$, $p=0.004$), and a post hoc Tukey test showed that antioxidant activity at high light was lower in western Mediterranean ecotypes than in central Asian and European ecotypes ($p\leq0.05$) (Fig. 2 C). The lower antioxidant activity in western Mediterranean ecotypes may indicate that these populations are less sensitive to high light perhaps by avoiding or counteracting oxidative damage via non-antioxidant mechanisms.

In Experiment 3, ecotypes under night freezing (~ –4ºC) had greater fresh mass ($F(1,300)=75.12$, $p<0.0001$), higher antioxidant activity ($F(1,300)=221.2$, $p<0.0001$), with greener (lower values of $PC1_{ExtractsColor}$, $F(1,339)=415.9$, $p<0.0001$) and redder extracts (lower values of $PC2_{ExtractsColor}$, $F(1,339)=12.07$, $p=0.0006$) than when grown with night-time temperatures just above freezing (2ºC grown sequentially in same chamber under high light, Fig. 2, right panels). Although plants were larger under night-time freezing, survival was significantly lower than under no freezing (76 vs 100%, $F(1,300)=273.2$, $p<0.0001$). Additionally, an ANOVA showed significant differences in $PC1_{ExtractsColor}$ under night-time freezing between regions (i.e., greenness of extracts; $F(3,160)=4.11$, $p=0.007$). A post hoc Tukey test found that ecotypes from eastern Africa had less green/more yellow extracts than ecotypes from other regions ($p=0.01$, Fig. 2F), potentially due to more xanthophylls and less chlorophylls.

We also examined significant ($p<0.05$) trait covariation and associations with performance globally and within regions (Fig. S2–S6). In Experiment 2, antioxidant activity under high light was globally correlated with darker (lower $PC1_{LeavesColor}$, $r= -0.22$, $p=0.01$) and bluer leaves (higher $PC2_{LeavesColor}$, $r=0.34$, $p<0.001$), suggesting pigments act as antioxidants. It is not clear, however, if more pigments and antioxidants are adaptive because none of these traits were correlated with survival. Only in central Asia, earlier flowering was associated with greater fresh mass ($r= -0.39$, $p=0.03$) and higher survival rates ($r= -0.48$, $p=0.01$) under high light, suggesting life history variation may be under selection.

In Experiment 3, the relationship between leaf extract color and antioxidant activity under night-time freezing was weak and unclear; globally, ecotypes with higher antioxidant activity were associated with less red extracts (higher values of $PC2_{ExtractsColor}$, $r= 0.19$, $p=0.03$). In western Mediterranean and eastern African ecotypes, higher plasticity in antioxidant activity

was associated with lower survival (r= -0.38, p<0.001, and r= -0.87, p=0.01 respectively). Furthermore, in these latter two regions, ecotypes with darker green extracts (lower values of $PC1_{ExtractsColor}$) had greater fresh mass (r= -0.33, p<0.001 in western Mediterranean and r= -0.69, p=0.01 in eastern Africa), and had higher survival rates in eastern Africa (r= -0.78, p<0.001) under night-time freezing. In western Mediterranean ecotypes, survival rates under night-time freezing were negatively associated with antioxidant activity (r= -0.27, p=0.02). In contrast, central Asian ecotypes with darker green extracts had greater fresh mass (r= -0.37, p=0.01) under night-time freezing. Thus, under night-time freezing, higher antioxidant activity and pigmentation may contribute together to higher fitness in central Asia, and greener pigmentation to higher fitness in eastern Africa and western Mediterranean. However, higher antioxidant activity and plasticity in antioxidant activity may be maladaptive and indicate a failure to maintain homeostasis in the latter two regions.

Figure 2. Significant phenotypic plasticity under contrasting light (Experiment 2–left) and contrasting night-time temperatures (Experiment 3–right), dots are means of breeding values and bars are standard errors colored by region. When present, different letters indicate significant differences between regions from a post-hoc Tukey HSD test (*p*<0.05). **A, B.** Fresh aboveground mass (mg). **C, D.** Antioxidant activity (ug/mg). **D, E** and **F, G**. Principal components 1 and 2 that come from percent and amount (respectively) of red, green, and blue lights obtained from a representative mid-aged leaf and leaf extract (respectively). In Experiment 2 central Asia N=32, Europe N=13, western Mediterranean N=63. In Experiment 3 central Asia N= 44, Europe N= 26, eastern Africa N=12, western Mediterranean N=69.

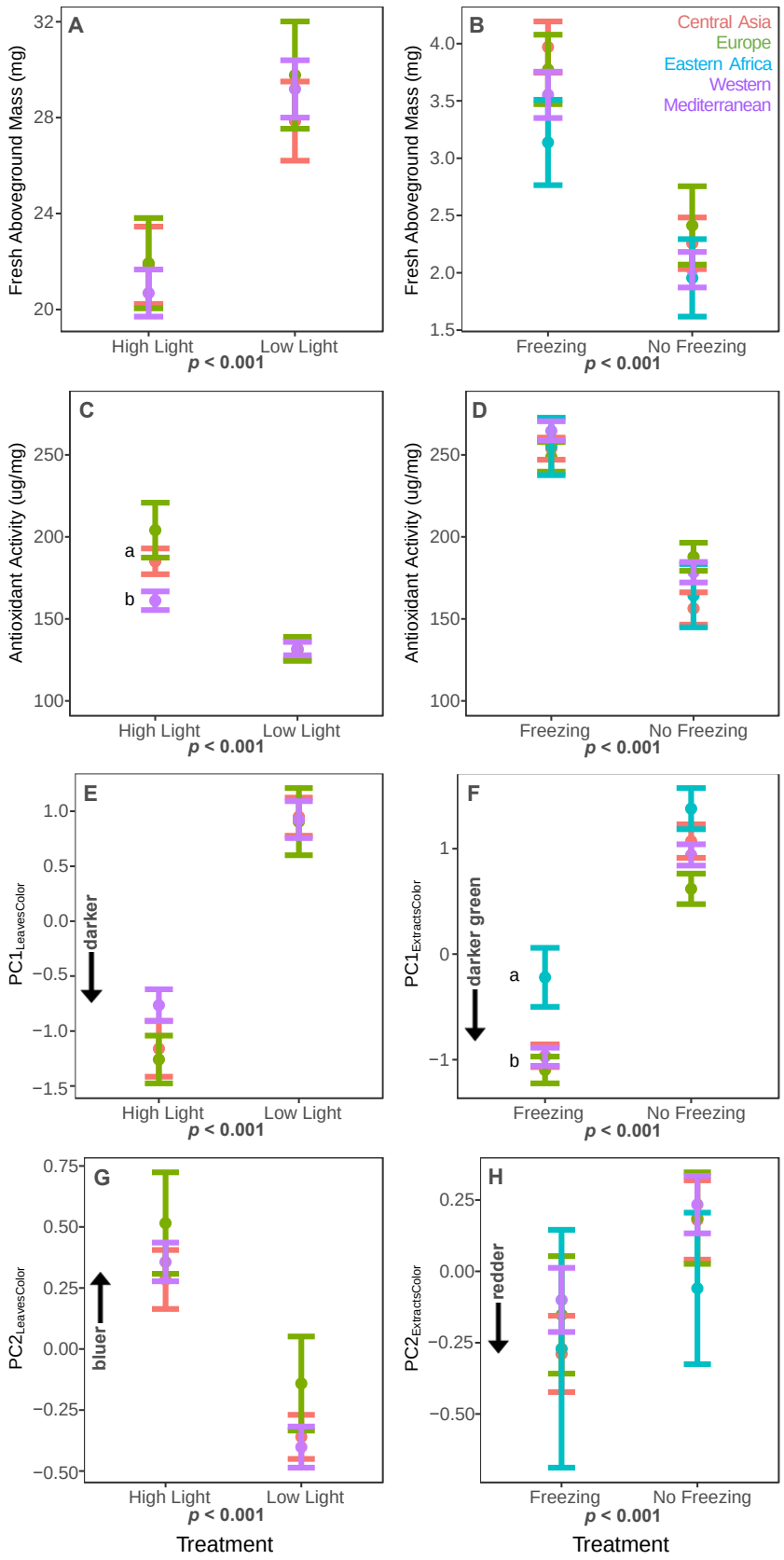
A
Fresh Aboveground Mass (mg)
32
28
24
20
High Light
Low Light
p < 0.001
B
Central Asia
Europe
Eastern Africa
Western
Mediterranean
Fresh Aboveground Mass (mg)
4.0
3.5
3.0
2.5
2.0
1.5
Freezing
No Freezing
p < 0.001
C
Antioxidant Activity (ug/mg)
250
200
150
100
a
b
High Light
Low Light
p < 0.001
D
Antioxidant Activity (ug/mg)
250
200
150
100
Freezing
No Freezing
p < 0.001
E
PC1LeavesColor
1.0
0.5
0.0
−0.5
−1.0
−1.5
darker
High Light
Low Light
p < 0.001
F
PC1ExtractsColor
1
0
−1
darker green
a
b
Freezing
No Freezing
p < 0.001
G
PC2LeavesColor
0.75
0.50
0.25
0.00
−0.25
−0.50
bluer
High Light
Low Light
p < 0.001
Treatment
H
PC2ExtractsColor
0.25
0.00
−0.25
−0.50
redder
Freezing
No Freezing
p < 0.001
Treatment

NPQ kinetics and photosynthesis

NPQ kinetics in response to fluctuating light (e.g., due to cloud changes) can be an important mechanism of limiting photooxidative damage. We carried out a set of detailed measurements of genetic variation in NPQ kinetics (dynamics through time) and photosynthesis in response to two potential abiotic stressors that vary with elevation (cold and drought; Fig 1E, F) on a global subset of 9–11 ecotypes (Table S1). In the first experiment, we grew plants in control (22°C) vs cold conditions (4°C). In the second experiment, we grew plants in control (no drought) vs experimental drought conditions (withholding watering for five days). In both experiments, we exposed plants to three sequential fluctuating light-dark cycles. In each cycle, we imaged dynamic changes in chlorophyll *a* fluorescence and fitted non-linear curves to individual NPQ time series to obtain six parameters (17 total across all light-dark cycles): initial NPQ prior to light exposure ($residual_{light}$) estimated only during the 2nd and 3rd cycle, rate of NPQ induction following light exposure ($time\ constant_{light}$), maximum value of NPQ estimated from the asymptote ($asymptote_{light}$), rate of NPQ relaxation after darkness ($time\ constant_{dark}$), minimum value of NPQ estimated from the asymptote ($asymptote_{dark}$), and final NPQ after darkness estimated from the distance between the asymptote and zero during recovery ($residual_{dark}$) (Fig. S7). We found no significant effect of cold or drought on the maximum quantum yield of photosystem II (F_v/F_m, $p \geq 0.83$ in both experiments; data not shown). In contrast, cold and drought significantly affected all NPQ kinetics' parameters analyzed (Tables S6–S7).

Cold generally promoted rapid NPQ induction ($residual_{light}$ in the 3rd cycle, $time\ constant_{light}$ and $asymptote_{light}$ in all three cycles: $p < 0.0001$) and to some degree NPQ relaxation ($residual_{dark}$ in the 3rd cycle, $time\ constant_{dark}$ in all 3 cycles, $asymptote_{dark}$ in the 2nd and 3rd cycles: $p \leq 0.007$). Drought also significantly affected the kinetics of NPQ induction ($residual_{light}$, $time\ constant_{light}$, $asymptote_{light}$ in all three cycles, $p \leq 0.04$) and relaxation ($asymptote_{dark}$ and $time\ constant_{dark}$ in all three cycles, $residual_{dark}$ in the 2nd and 3rd cycles, $p \leq 0.05$), but its effects were less pronounced than cold and greatly variable between ecotypes (Fig. 3). We detected significant genetic variation in all parameters in both experiments, and a significant interaction of ecotype by treatment for 11 cold-experiment and all drought-experiment parameters (Table S6–S7, Fig. S8–S9), but this variation was not clearly related to elevation of origin.

Among all ecotypes, CYR from low and seasonally dry central France showed no NPQ response to cold but the strongest response to drought. Conversely, Dja-1 from high and cold Central Asia showed no response to drought but the strongest response to cold (Fig. 3). JL-011-2-1 from tropical alpine eastern Africa and the naturalized Col-0 also showed rapid NPQ induction due to cold in all three cycles (Fig. S8 G-I), and Pi-0 from highland Alps showed the most rapid NPQ induction due to drought in all three cycles (Fig. S9 G-I). In IP-Trs-0, the only ecotype carrying the alternate allele for PHT4;4 in this set of experiments (locus identified below in GWAS), cold and drought had a similar effect of slight and mostly insignificant increases in NPQ kinetics across all three light-dark cycles (Fig. 3), suggesting reduced sensitivity to these abiotic stressors in this rapid-flowering low elevation Spanish ecotype.

Figure 3. Representative examples of NPQ curves during three sequential light-dark cycles in cold- (left panels) and drought- (right panels) treated plants and corresponding control. **A**, **E**. Sij-1; **B**, **F**. Dja-1; **C**, **G**. IP-Trs-0; **D**, **H**. CYR. Error bars indicate SEM (N cold=6 replicates; N drought=9–10 replicates, 5 in Dja-1).

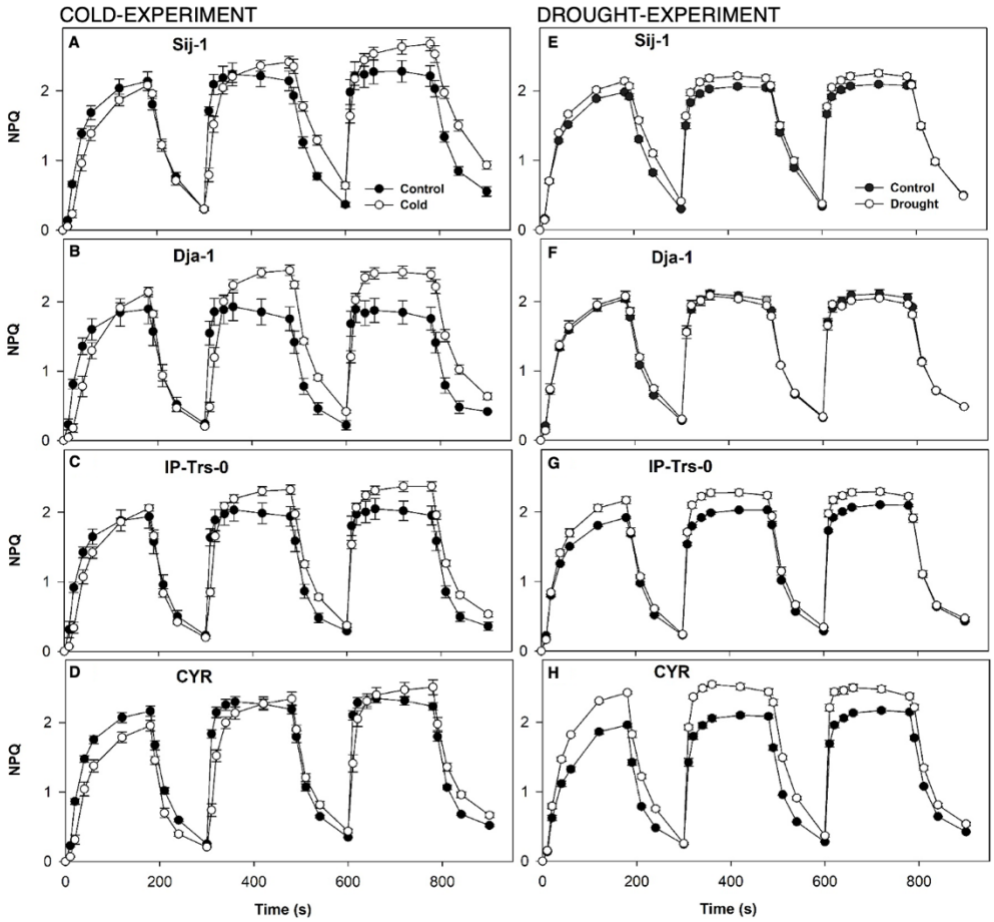

On a subset of eight ecotypes, we also found significant genetic variation in photosynthetic parameters measured at: 1) steady-light-states during gradual increases of light intensity from 0 to 1000 μmol m^{-2} s^{-1} waiting until a steady state at each light level (Table S8) and 2) fluctuating-light-states during a light regime that went from 1000 to 0 μmol m^{-2} s^{-1} waiting for 4 min at 1000 before each light-intensity change. To directly compare photosynthetic parameters with leaf pigment composition, we also examined chlorophylls *a*, *b*, and total carotenoids, finding significant differences among ecotypes (Table S9). As in NPQ experiments, there was no clear relationship with elevation of origin. Notably, Dja-1 and Sij-1 from similar environments in high Central Asia showed very contrasting values of photosynthetic parameters: Dja-1 had the greatest photosynthetic capacity and pigment content, while Sij-1 had the lowest photosynthetic capacity, potentially due to a significantly lower total carotenoid content. The Afroalpine ecotype JL-011-2-1 showed intermediate values of photosynthetic capacity, but the lowest pigment content together with the lowest *a* to *b* chlorophyll ratio and the highest chlorophylls to total carotenoids ratio.

Finally, we examined fresh and dry weighs in the subset of 11 ecotypes studied for NPQ kinetics (Fig. S10). Interestingly, JL-011-2-1 and IP-Trs-0 had the lowest fresh weight and the highest dry matter content (~64% of the fresh weight), indicating low water content. Dij-1 also showed a similar but less prominent pattern (dry matter content was ~32% of fresh weight), while for the rest of ecotypes dry matter content was ~20% of fresh weight (Fig. S10 B–D).

Elevational clines in phenotype

To understand how different elevational gradients shape phenotypic variation, we tested for region-specific trait-elevation associations. For traits that significantly varied with elevation, we performed linear mixed models that controlled for genome-wide similarity among ecotypes. Across experiments and regions, 17 out of 119 trait-elevational clines were nominally significant ($p<0.05$), 11 were significant with FDR = 0.05, and 9 were significant after accounting for genetic relatedness (Tables S10–S12), suggesting selection maintains those clines. Additionally, 11 out of 36 traits showed significant differences among regions (Supplemental Results 2, Table S13). The significant (FDR≤0.5) trait-elevation relationships presented below were different between regions.

In the western Mediterranean, days to flower (at 10 and 16ºC; $F(1,90)=22.98$ and $F(1,84)=12.73$, respectively), rosette compactness ($F(1,110)=30.66$), $\delta^{13}C$ ($F(1,108)=44.63$), $PC1_{Exp1}$ ($F(1,83)=23.62$), $PC2_{Exp1}$ ($F(1,83)=9.03$), and fresh mass under high and low light ($F(1,61)=18.23$ and $F(1,63)=8.46$, respectively) were positively associated with elevation (Fig. 4 and 5). These clines remained significant in a mixed model accounting for genetic relatedness among ecotypes ($p\leq0.03$). Thus, ecotypes from higher elevations in the western Mediterranean displayed late flowering, higher water use efficiency, and more compact rosettes with greater fresh mass.

In contrast, ecotypes from central Asia flowered earlier at higher elevations ($F(1,73)=23.9$ and 23.8 for days to flower at 10 and 16ºC, respectively), with $PC1_{Exp1}$ also being negatively associated with elevation ($F(1,71)=12.45$). Ecotypes from higher elevations also tended to have greater fresh mass under high and low light, but this trend was only nominally significant ($F(1,29)=9.93$ and $F(1,31)=8.64$, for high and low light respectively, $p<0.01$, FDR = 0.08). Furthermore, after accounting for population genetic structure, flowering time was no longer significantly associated with elevation ($p=0.2$ and $p\geq0.06$ for days to flower at 10 and 16ºC respectively; Table S12), making unclear whether flowering time is under selection.

In Europe, no relationship passed FDR, though nominally significant clines included greater rosette diameter ($F(1,53)=9.39$), stomatal length ($F(1,21)=6.25$) and leaf C:N ($F(1,53)=4.8$) with increasing elevation ($p\leq0.03$). We found no significant elevational clines in traits at FDR=0.05 in Experiment 3 for any region (Fig. S11). Although antioxidant activity seemed to increase with elevation in eastern Africa under night-time freezing, we had only 11 ecotypes and this trend was not significant ($F(1,9)=4.27$, $p=0.07$). In neither experiment and/or region were significant patterns revealed for plasticity in pigmentation and elevation (Figs. S2–S6).

Finally, to understand how different environmental factors along elevation affect phenotypic variation, we tested for associations between traits and selected environmental variables that vary with elevation (Table S10). They involved growing season variables, including length, moisture (aridity index), and night-time temperature (minimum temperature), and isothermality (day: year temperature ratio). Most significant (FDR≤0.05) phenotype-environment associations were in central Asia and affected flowering time: later flowering was associated with longer growing seasons ($F(1,73)=15.38$) and lower isothermality ($F(1,73)=11.37$), which in turn are more common at lower elevations (Fig. 1 D, G). In contrast, in the western Mediterranean later flowering was associated with lower night-time temperatures during the growing season ($F(1,90)=12.93$), which are more common at higher elevations (Fig. 1 F). Thus, despite similar environment-elevation clines between central Asia and the western Mediterranean (Fig. 1 D–G), the environmental factors along elevation that influence phenotypic

variation are different in each region. In Europe, isothermality also significantly influenced several traits (FDR≤0.05), including flowering time: as in central Asia, later flowering was associated with lower isothermality (F(1,47)=57.35), but isothermality was rather weakly correlated with elevation in Europe (Fig. 1 G).

Figure 4. Linear regressions of several phenotypes from Experiment 1, and flowering time, on elevation of origin. Ecotypes and fitted lines are colored by region: central Asia in red N=74–76, Europe in green N=48–55, and western Mediterranean in purple N=85–112. Relationships with FDR<0.05 are depicted with their corresponding adjusted-R^2, which are bolded when $p \leq 0.05$ in linear mixed-effects kinship models. **A**. Days to flower at 16 ºC obtained from the 1001 Genomes Consortium (Alonso-Blanco et al., 2016). **B**–**F** Traits measured in Experiment 1. **G**–**H** PC1 and PC2 of traits measured in Experiment 1 and flowering time (grown at 10 and 16 ºC).

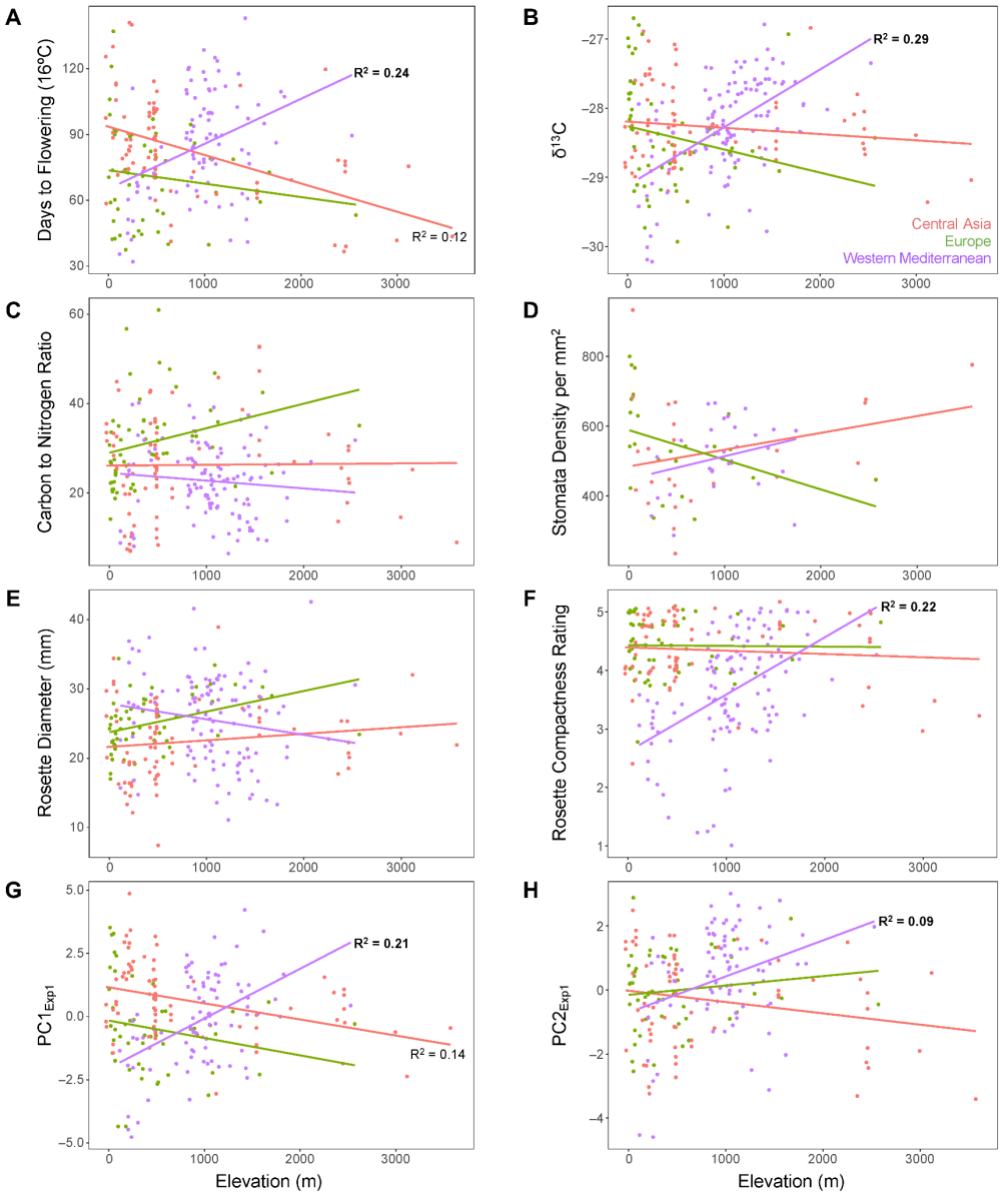

Figure 5. Linear regressions of phenotypes measured in Experiment 2 on elevation of origin. Left panels are traits measured under high light and right panels under low light. Ecotypes and fitted lines are colored by region: central Asia in red N=74–76, Europe in green N=48–55, and western Mediterranean in purple N=85–112. Relationships with FDR<0.05 are depicted with corresponding adjusted-R^2, which are bolded when $p \leq 0.05$ in linear mixed-effects kinship models. **A**, **B**. Fresh aboveground mass (mg). **C**, **D**. Antioxidant activity (ug/mg). **E**, **F**. PC1 of leaf color. **G**, **H**. PC2 of leaf color. **I**. Plasticity in antioxidant activity (ug/mg). **J**. Survival rate under high light (most stressful treatment).

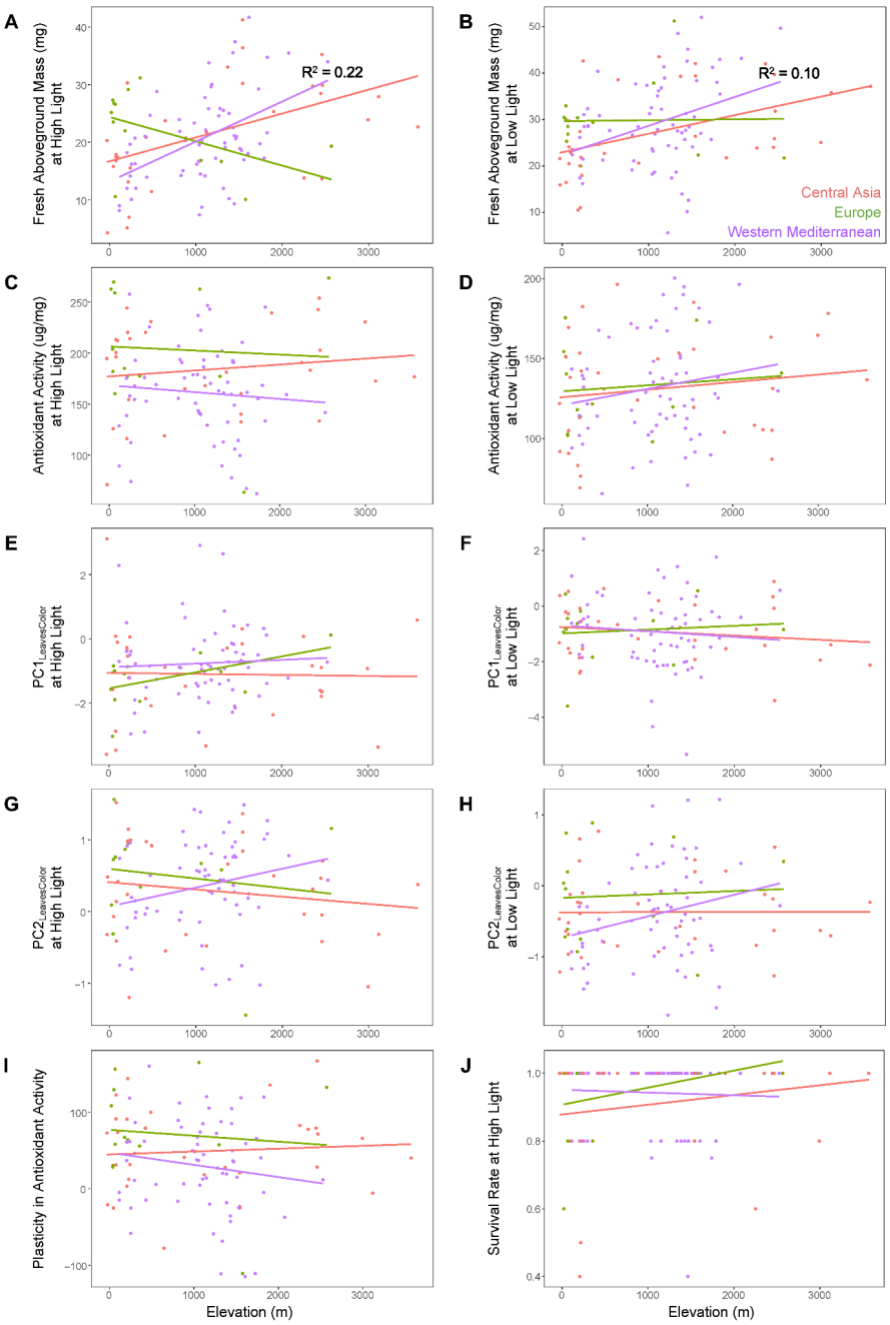

Genomic basis of trait variation

We performed mixed-model genome wide association studies (GWAS) with between ~2.0–2.4M SNPs filtered for minor allele frequency (MAF>0.05), while controlling for genome-wide similarity among ecotypes (Tables S14–S18). We included traits for which we had observations from three or more replicates. GWAS were performed on our global dataset (N=110–253 ecotypes), and on regional datasets for traits that significantly varied with elevation (N=32–192). We highlight strong candidate protein coding genes whose annotated function relates to that trait function (Fig. 6).

Genes underlying later flowering and higher $\delta^{13}C$ at higher elevations in the western Mediterranean

In the western Mediterranean, we found significant QTL for flowering time and $\delta^{13}C$ (Fig. 6 A–B, E–G, FDR < 0.05). For flowering time, the top QTL (grown at 16ºC) and the 3rd top QTL (grown at 10ºC) was *DOG1* (*Delay of Germination 1*), an extensively studied gene involved in regulating seed dormancy and flowering time (Graeber et al., 2014; Huo et al., 2016; Alonso-Blanco et al., 2016; Martínez-Berdeja et al., 2020). The top SNP in the *DOG1* QTL (chr5: 18590591) was also significantly associated with elevation: its alternate allele was involved in late flowering and restricted to high elevation, suggesting a locally adaptive elevational cline in this *DOG1* variant (Fig. 7 A–C, Table S18). This SNP was previously identified by Martínez-Berdeja (2020) because of its association with germination, and the alternate allele tags some (15 of 52 in Iberia and 15 of 68 in Morocco) of the genotypes carrying the ancestral haplotype of the self-binding domain (ECCY). Thus, the top SNP in the *DOG1* QTL segregates in ecotypes carrying the ECCY haplotype in Morocco and Iberia, but not other haplotypes which all carry the reference allele. In the widely distributed ECCY haplotype germination is more common in the fall via cold-induced dormancy (Martínez-Berdeja et al. 2020). These plants exhibit a winter-cycle late-flowering strategy, where they overwinter as small rosettes, flowering in the spring after strict vernalization requirements (Exposito-Alonso 2020).

Martínez-Berdeja (2020) noted global climatic associations between *DOG1* haplotypes in the functional domain, including elevation, but did not characterize the direction of elevational clines. Here, we found that haplotype variation identified by Martínez-Berdeja (2020) in *DOG1* was region specific: haplotype frequency was strongly associated with elevation in the western Mediterranean (Kruskal-Wallis chi^2=36.24, df=4, p<0.0001) and Europe (Kruskal-Wallis chi^2=77.21, df=2, p<0.0001), but not in central Asia (Kruskal-Wallis chi^2=0.75, df=1, p=0.39) (Fig. S12, left panels). Relative to other haplotypes, ECCY was associated with higher elevations in the western Mediterranean, but with lower elevations in Europe. Nevertheless, compared to other haplotypes ECCY was associated with late flowering in all regions (Kruskal-Wallis chi^2=52.73, df=4, p<0.0001 in the western Mediterranean, Kruskal-Wallis chi^2=116.55, df=2, p<0.0001 in Europe, Kruskal-Wallis chi^2=13.32, df=1, p=0.0003 in central Asia; Fig. S12, right panels). Thus, the role of *DOG1* haplotype variation in local adaptation along elevational gradients likely differs from region to region.

For $\delta^{13}C$, the top (number 1) and the 9th top QTL were upstream (in the putative promoter region) of two genes involved in regulation of abscisic acid (ABA) in response to osmotic stress (Fig. 6 E–G). The first is *Nicotinamidase 3* (*NIC3*), which encodes an enzyme that prevents the accumulation of intracellular nicotinamide by converting it into nicotinic acid in the NAD+ pathway, and which is expressed via Repressor of Silencing 1 (ROS1) DNA demethylation in response to ABA (Kim et al., 2019). The other is *MAP3 kinase* (*MAP3k*), which is involved in

the phosphorylation of SnRK2 kinases that in turn trigger osmotic-stress and ABA responses (Takahashi et al., 2020). The top SNPs in these QTL (chr5: 7822318 for *NIC3* and chr5: 3831491 for *MAP3k*) were also strongly associated with elevation of origin: the reference alleles were associated with higher $\delta^{13}C$ and elevation (Fig. 7 G–I, Table S18), suggesting that changing selection with elevation on *NIC3* and *MAP3k* expression contributes to elevational clines in $\delta^{13}C$ via the ABA pathway and stomatal conductance. We note that the alternate allele of these two SNPs was almost completely restricted to low elevation sites in the Iberian Peninsula (allele frequency (af)=0.14 for chr5: 7822318 and af=0.08 for chr5: 3831491 in the Iberian Peninsula) (Fig. 7 G), where summers are hot and dry and associate with a rapid-cycling earlier flowering strategy (Wolfe and Tonsor, 2014; Exposito-Alonso, 2020).

The genetic basis of elevational clines in flowering time in central Asia

In central Asia, no SNP passed FDR≤0.05. For flowering time (at 16ºC) the 7th top QTL was in the putative promoter region of a MADS-box protein encoded by the *Flowering Locus C* (*FLC*) gene (Fig. 6 B). *FLC* is well-studied, represses floral transition, and is downregulated through epigenetic silencing induced by vernalization, *FRIGIDA*, or the autonomous pathway (Hepworth et al., 2020; Deng et al., 2011). Studies in other regions (global and in the western Mediterranean) have shown environmental clines in *cis*-regulatory elements of *FLC* (Sánchez-Bermejo et al., 2012; Li et al., 2014; Méndez-Vigo et al., 2016; Hepworth et al., 2020). Here we found that the alternate allele of the top SNP in this QTL (chr5: 3180228) was almost restricted to the Caucasus (af=0.18) (Fig. 7 D–F), but unrelated to elevation there or across central Asia, despite the observed trend of earlier flowering at higher elevations. That alternate allele was also present in both Caucasus genetic clusters, suggesting admixture or shared ancestral variation (see Fig. 1 A).

Moroccan montane populations harbor alleles related to low antioxidant activity under high light independent from elevation

Globally, the top QTL associated with antioxidant activity under high light was adjacent to a gene involved in oxidative regulation induced by high light (Fig. 6 H–I). This gene encodes an inorganic phosphate transporter (*PHT4;4*) that transports ascorbate, an antioxidant, from the envelope membrane into the chloroplast, and its expression is induced by high light stress (Miyaji et al., 2015). Ascorbate is itself an antioxidant and is also important in the xanthophyll cycle and may be required for tolerance to high light (Miyagi et al., 2015). The top SNP's (chr4: 160735) allele associated with low antioxidants is globally uncommon but is dominant (af=0.82) in the high elevation (all but one ecotype >1000 m) Moroccan populations and rare (af=0.03) in the nearby low elevation Iberian populations. This SNP explained 40% of the variation in antioxidant activity under high light in Morocco, and 42% in the greater western Mediterranean. Moreover, we calculated F_{ST} values for all SNPs in chromosome 4 (where *PHT4;4* is located) comparing Morocco to the rest of Eurasian genotypes. The QTL at *PHT4;4* (chr4: 160735) has an F_{ST} of 0.1944 (Table S19), which is in the 0.005 tail for the SNPs on the chromosome, suggesting that this variant is locally adaptive in Morocco. However, we did not find an elevational trend in that SNP within Morocco nor in the greater Western Mediterranean (Fig. 6 J–L), consistent with our finding of no strong antioxidant-elevation trend. Indeed, *PHT4;4* knockouts had reduced levels of ascorbate in leaves when exposed to high light compared to controls, and this was associated with reduced production of xanthophylls and beta-carotenes (Miyagi et al., 2015). We found the *PHT4;4* antioxidant SNP was also associated with pigments

in a way consistent with the findings of Miyagi et al. (2015). Specifically, we found that the allelic variant related with low antioxidant activity (dominant in Morocco) was also significantly associated with lighter leaves and leaf extracts (i.e., higher values of $PC1_{LeavesColor}$ and $PC1_{ExtractsColor}$) in our high light (t=3.3, df=41.8, p=0.002), night-freezing (t=2.2, df=19.5, p=0.04) and no night-freezing experiments (t=2.4, df=16.9, p=0.03), but not in the low light experiment, consistent with Miyagi's (2015) finding of *PHT4;4* knockout effects being conditioned on high light. Our findings suggest that the Moroccan allele tags a locally adapted reduced function variant of *PHT4;4*.

The second top QTL associated with antioxidant activity under high light tagged the *Ferric Reduction Oxidase 7* (*FRO7*) gene (Fig. 6 J), which is involved in iron transport from the cytosol into the chloroplast during photosynthesis (Jeong and Connolly, 2009), especially in cotyledons (Jeong et al., 2008). Like *PHT4;4*, the allelic variant of the top SNP (chr5: 20206030) associated with lower antioxidant activity was common in Morocco (af=0.78), while less common in Iberia (af=0.08) and elsewhere (af=0.04), and it did not vary with elevation (p=0.9).

The distribution of p-values in the GWAS of antioxidant activity under high light was right-skewed, with an excess of low p-values, suggesting incomplete control of population structure. This excess was likely driven by under-fitting the genomic background effect (kinship random effects) for the genetically distinct Moroccan genotypes (Atlas Mountains in Fig. 1 B) that also had low antioxidant activity (Fig. 7 K). We thus performed another GWAS on this trait by incorporating a covariate that indicated if the accession belonged to the distantly related Moroccan lineage. P-values on this GWAS were higher (FDR=0.9 for all; Table S15), SNPs in *PHT4;4* were no longer among the top 25 and one SNP in *FRO7* (chr5: 20206030) was in the 13th top QTL. We note that for *PHT4;4*, only one accession outside Morocco carrying the low antioxidant allele was phenotyped, indicating that finding *PHT4;4* in our original global GWAS was solely driven by Moroccan ecotypes.

Figure 6. Genome-wide association studies (GWAS) of selected traits. Left panels show Manhattan plots over the Arabidopsis genome with top hit SNPs marked in red when close to genes, or in green when inside genes. Right panels are zoomed-in on candidate gene QTL, where SNPs in candidate genes (showing their strand) are marked in green, and close-by top SNPs marked in red. The dashed line in plots corresponds to a genome-wide Bonferroni threshold of *p*=2.5e-8. SNPs were filtered for MAF=0.05. **A**–**B**. N=183, 2'142,456 SNPs. **C**–**D**. N=109, 1'985,124 SNPs. **E**–**G**. N=110, 2'290,321 SNPs. **H**–**J**. N=110, 2'302,985 SNPs.

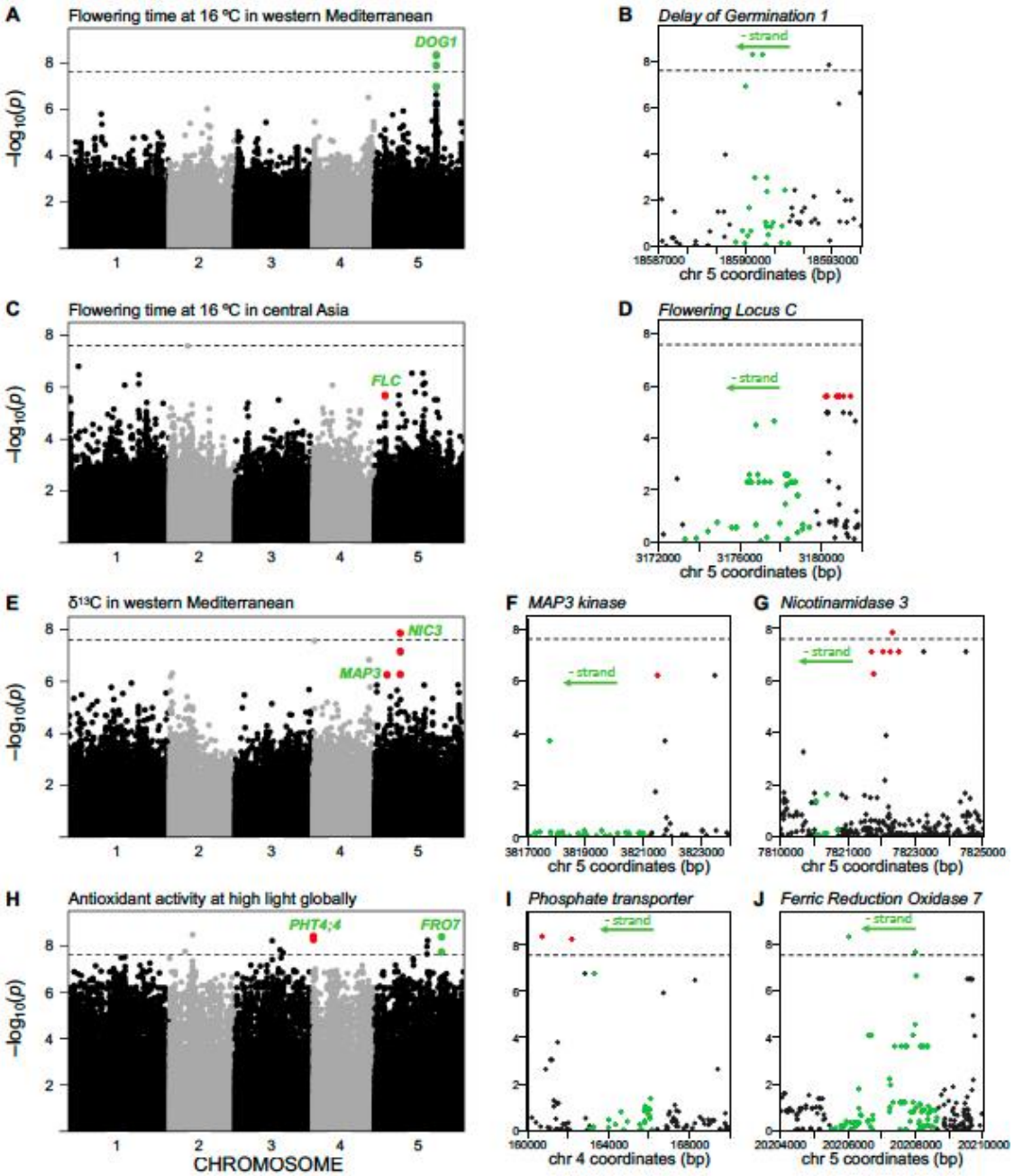
A
Flowering time at 16 °C in western Mediterranean
DOG1
B
Delay of Germination 1
- strand
chr 5 coordinates (bp)
C
Flowering time at 16 °C in central Asia
FLC
D
Flowering Locus C
- strand
chr 5 coordinates (bp)
E
δ13C in western Mediterranean
NIC3
MAP3
F
MAP3 kinase
- strand
chr 5 coordinates (bp)
G
Nicotinamidase 3
- strand
chr 5 coordinates (bp)
H
Antioxidant activity at high light globally
PHT4;4
FRO7
CHROMOSOME
I
Phosphate transporter
- strand
chr 4 coordinates (bp)
J
Ferric Reduction Oxidase 7
- strand
chr 5 coordinates (bp)
−log10(p)

Figure 7. Geographic distribution (left panels) and variation of top SNP variants relative to traits of interest (middle panels), and elevation (right panels) in **A**–**C**. *Delay of Germination 1* (*DOG1*). **D**–**F**. *Flowering Locus C* (*FLC*). **G**–**I**. *Nicotinamidase 3* (*NIC3*), and **J**–**L**. *Inorganic Phosphate Transporter 4* (*PHT4;4*). Boxplot width is proportional to allele frequency.

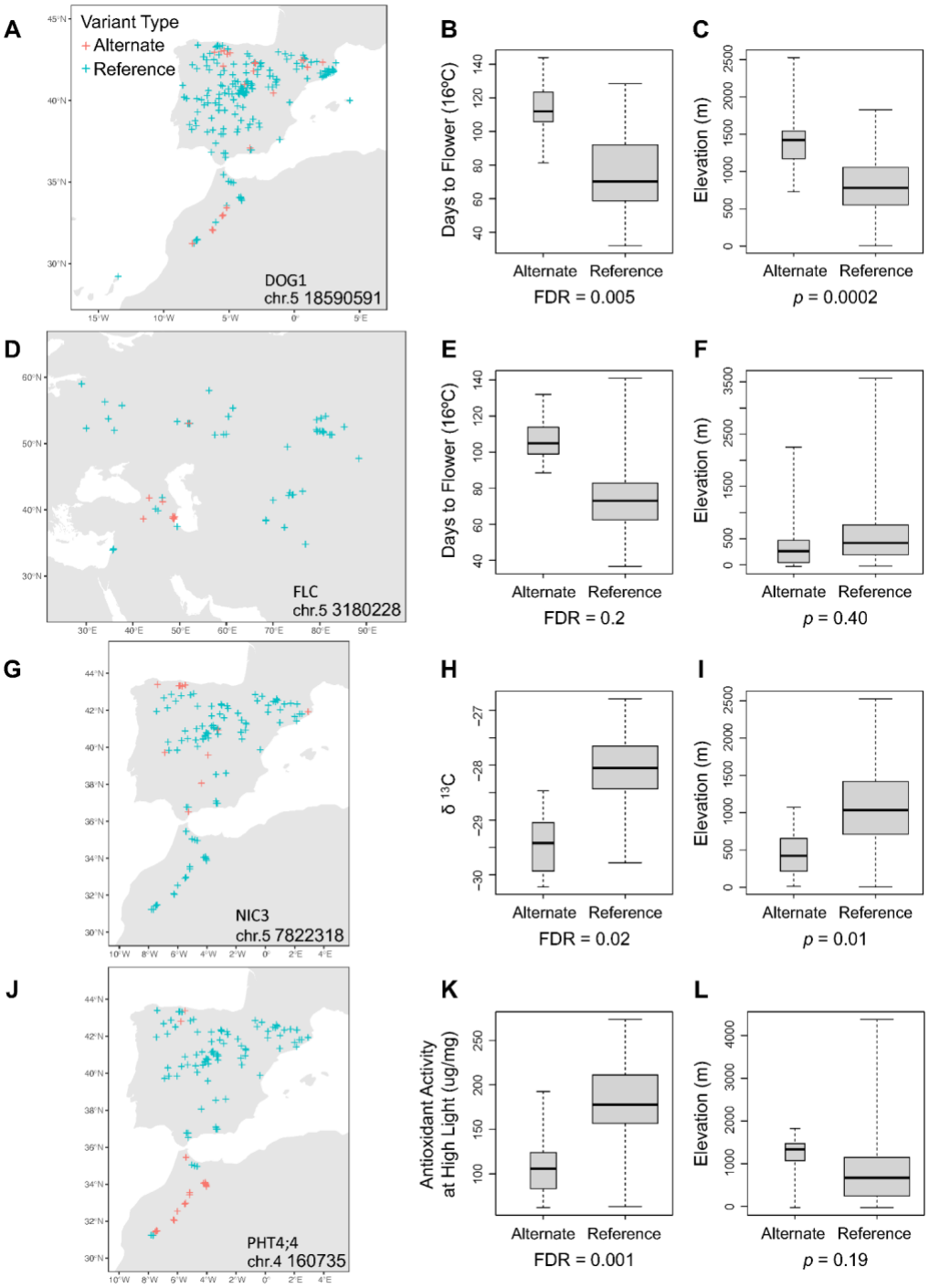

Discussion

Arabidopsis exhibits natural genetic variation in abiotic stress response, which is in turn often linked to seasonal timing and structured along elevational gradients. Germination and flowering time show evidence of local adaptation partly in response to seasonal cold at high elevations (Méndez-Vigo et al., 2011; Suter et al., 2014; Vidigal et al., 2016). Biomass and morphology also change with elevation in Arabidopsis, with plants often presenting 'alpine dwarfism' and succulence at high elevations in some regions (Luo et al., 2015a, 2015b). Moreover, water use efficiency (WUE) and its genetic basis may be associated with phenology (Lovell et al., 2013; Kenney et al., 2014), though changes in WUE with elevation have been less clear in the literature (Dittberner et al., 2018; but see Wolfe and Tonsor, 2014). Some elevational clines in genotype and genetic variation in phenotypes have been identified (Tyagi et al., 2016; Tripathi et al., 2019; Singh and Roy, 2017). However, past studies of elevational clines have focused on individual geographic regions in Eurasia, precluding a broader understanding of adaptation to global elevational gradients.

Here we took a multi-regional approach to examine the genomics and physiology of adaptation to elevation of *Arabidopsis thaliana* in its native range. We uncovered elevational clines suggesting changing selection for several traits. Notably, all elevational clines were region-specific; there were no global elevational clines despite some global similarities in environmental gradients. Phenotype variation differed among regions, and the association of traits to survival (an aspect of fitness) was, in some instances, region-specific. Antioxidant activity, pigmentation, photosynthesis, and NPQ kinetics all showed substantial genetic variation, but it was not clearly linked with elevation. With one exception (Caucasus), we found that population genomic structure was associated with geography and not elevation (e.g., as described in Afroalpine *Dendrosenecio*, (Tusiime et al., 2020). This pattern suggests that even when selective gradients are consistent among mountain ranges, local adaptation may occur in parallel. Below we discuss the elevational clines we did identify, as well as regional phenotypic differences, and putative causal genetic loci.

An elevational cline in life history and physiology in the Western Mediterranean

In the western Mediterranean we found an elevational cline in life history and water use efficiency potentially influenced by drought at low elevations. Low elevation ecotypes had open/spread out rosettes associated with a rapid-cycling strategy (early flowering) allowing drought escape, while high elevation ecotypes had compact rosettes associated with efficient water use (high $\delta^{13}C$) suggesting drought avoidance (Ludlow, 1989). The genetic basis of this cline may involve allelic variation in the seed dormancy/flowering time *DOG1* gene (Huo et al., 2016; Graeber et al., 2014), and in two candidate genes related to abiotic stress response in the ABA pathway, *MAP3k* and *NIC3* (Takahashi et al., 2020; Kim et al., 2019). Previous studies in the Spanish Pyrenees have also suggested that earlier flowering allows drought-escape in the lowlands (Montesinos-Navarro et al., 2011; Montesinos et al., 2009; Wolfe and Tonsor, 2014), and our results indicate that this strategy may also involve evolution of ABA signaling. Ecotypes from high elevation have alleles that allow them to counteract water loss under stress, but not those from low elevations in the western Mediterranean which are probably less commonly exposed to environmental stress during the growing season because of their rapid cycle (Exposito-Alonso, 2020).

Our findings also shed new light on the role of *DOG1* haplotypes in elevational adaptation, where variants of our top SNP in the *DOG1* QTL significantly changed with

elevation in the western Mediterranean but not in other regions. The ancestral ECCY haplotype, which is associated with a winter-annual life cycle (Exposito-Alonso, 2020) is dominant at high elevations in western Mediterranean ecotypes. Plants carrying the ECCY haplotype germinate in the fall due to low germination rates after cold periods, and long periods of cold temperatures are required to induce flowering. Ecotypes carrying derived haplotypes (D-RY, D-SY, ECSY, and EFSY), that are more common at low elevations, germinate in the spring in response to the end of cold periods, or have secondary seed dormancy that is released with warm temperatures, and cold temperatures are not required to induce flowering (Martínez-Berdeja et al., 2020; Exposito-Alonso, 2020).

Wolfe and Tonsor (2014) found that instantaneous water use efficiency of flowering Arabidopsis was higher for ecotypes from lower elevations under hot and dry conditions. Instantaneous measurements are indicative of short-term acclimation to drought stress but are not integrated across time like carbon stable isotope ratio, $\delta^{13}C$ is (Des Marais et al., 2014), thus they might not give a full picture of water use efficiency (Mckay et al., 2003). Moreover, in wild-collected Arabidopsis herbarium specimens, discrimination against ^{13}C ($\Delta^{13}C$) was indeed lower, indicating higher WUE, at higher elevations, but this pattern was strongest in eastern Europe and central Asia, while non-significant in the western Mediterranean (DeLeo et al., 2020). More studies are needed to understand how water use efficiency may vary across the entire life cycle of Arabidopsis and to estimate how different proxies inform physiological responses to dehydration stress.

Earlier flowering at higher elevations in central Asia

In central Asia, results suggest a rapid-cycling strategy may be adaptive under cool high light conditions with short growing seasons at high elevations. We found earlier flowering was related to higher survival and greater fresh mass under high (but not low) light experimental conditions, with a tendency of greater fresh mass in ecotypes from higher elevations. Furthermore, ecotypes from locations with shorter growing seasons and higher isothermality (i.e., lower day: annual variation) had faster flowering, and growing seasons were shorter compared to other regions. Variation underlying this phenological-elevational cline, however, disappeared after correcting for genetic relatedness among ecotypes, making unclear if the cline is adaptive and consistent with the major turnover in genetic background with elevation in the Caucasus. Past studies from the western Himalayas suggest that changing light intensity with elevation influences natural phenotypic and genomic variation (Tyagi et al., 2016; Singh and Roy, 2017; Tripathi et al., 2019). It could thus be that in central Asia, earlier flowering is critical for escaping stressful conditions associated with high light at high elevation, but further studies are needed to determine if flowering time variation along elevation is indeed adaptive.

Trait variation along elevation is unclear in Europe

We did not find significant (FDR>0.05) elevational clines in our European region. Other studies along elevational gradients in Europe have also failed to find strong phenotypic clines, sometimes despite genomic signatures of local selective sweeps in regions related to stress response (see Günther et al., 2016). For example, in the north Italian Alps phenotypic variation in frost and UV tolerance was correlated with population genetic structure between low and high elevation sites, making it unclear if selection maintains phenotypic variation (Günther et al., 2016). Also, differences in the number of frost days at a small geographic scale, and not elevation, were the best predictor of adaptive variation (i.e., frost hardiness) in the southern Alps

(Lampei et al., 2019). Understanding demographic histories along with microclimatic variation (see Frachon et al., 2018) will help clarify how elevational clines influence adaptive variation in Europe.

Antioxidant activity and pigmentation vary independent from elevation

While ecotypes showed shared increases in antioxidants and pigmentation changes in response to bright light and night-time freezing, and genetic variation in these traits differed among regions, it was not associated with elevation of origin. One explanation for the lack of clines is that high light levels cause more oxidative stress at lower temperatures, but drought also results in stress that is counteracted with accumulation of flavonoids such as anthocyanins (Nakabayashi et al., 2014). Thus, higher antioxidant activity might also be involved in local adaptation to drought.

Afroalpine populations occupy an outlier environment with respect to clear sky radiation and night-time cold throughout the year. While these ecotypes were not distinct in antioxidant activity, under night-time freezing eastern African ecotypes presented leaf extracts that were yellower compared to the dark orange and deep red extracts in other regions, potentially indicating carotenoids used in NPQ (Havaux and Kloppstech, 2001; Havaux et al., 2007). Interestingly, only in east African ecotypes, yellower extracts and higher plasticity in pigmentation were associated with higher survival under night-time freezing, suggesting potential selection on pigments. Additionally, a high elevation Afroalpine ecotype was very small, but had distinctly high leaf dry matter content measured in the photosynthesis and NPQ experiment, which might be adaptive if it enhances freezing resistance (Gorsuch et al., 2010).

Among western Mediterranean ecotypes, greater antioxidant activity and plasticity in antioxidant activity were associated with lower survival under night-time freezing. It may be that night-time freezing at high elevations is counteracted by other means than producing antioxidants, which in turn may be a sign of a failure to maintain redox homeostasis (i.e., maladaptive plasticity). For example, freezing tolerance was independent from antioxidant production in four European ecotypes that differ in cold tolerance (Distelbarth et al., 2013). Previous evidence on a small global dataset, however, suggested a positive correlation between freezing tolerance and activation of the flavonoid metabolism (Hannah et al., 2016). The lack of agreement between studies emphasizes the importance of regional differences in elevational selective gradients and resulting phenotypic and genetic clines.

Furthermore, under bright and cool conditions, western Mediterranean ecotypes had the lowest antioxidant activity. This pattern was driven by Moroccan ecotypes, which might exhibit lower sensitivity to high light and lower levels of ascorbate. These ecotypes have almost exclusively alleles at a transporter gene for ascorbate into the chloroplast (*PHT4;4*) associated with lower antioxidant activity (Fig. 6 J, K). The level of expression in this candidate gene increases with light exposure (Miyaji et al., 2015). Ascorbate is used in the xanthophyll cycle which in turn causes NPQ. Moroccan ecotypes might thus use NPQ mechanisms independent from the xanthophyll cycle, or from antioxidant activity altogether. IP-Trs-0, which carries the *PHT4;4* allele associated with low antioxidant activity, showed relatively low sensitivity in NPQ kinetics in response to cold or drought. Interestingly, Miyaji et al. 2015 found that *PHT4;4* knockouts under high light had lower levels of ascorbate in leaves, as well as reduced heat dissipation from excess light absorption, and reduced levels of xanthophyll and beta-carotene pigments, but these reductions were not associated with reductions in biomass. Thus, fitness in the non-functional *PHT4;4* mutants did not seem compromised.

NPQ kinetics and photosynthesis vary independent from elevation

We found significant genetic variation in NPQ kinetics and photosynthesis parameters, but this variation was not clearly related to elevation. The magnitude of differences in NPQ parameters between control and stress conditions was comparable to a previous study (Rungrat et al., 2019), but stress was probably not severe enough to induce photoinhibition (i.e., *Fv/Fm* was not significantly affected by cold or drought in our study). Rungrat et al. (2019) showed that NPQ kinetics were influenced by diurnal fluctuation in temperature and higher light intensity induced faster NPQ. Here we also show that cold and drought resulted in faster NPQ induction and relaxation, but this was highly variable among ecotypes and not exclusive to high elevation ones, potentially because cold and drought can happen at different elevations in different regions. NPQ can remove over 75% of absorbed light energy (Niyogi et al., 1998), thus its fast induction in response to stress can play an essential role for rapid defense against photoinhibition, preventing photodamage of the photosynthetic machinery by reducing ROS formation (Malnoë, 2018). Fast relaxation of NPQ (particularly evident in two Central Asian highland ecotypes) can also be vital because it allows more energy to be photochemically quenched under fluctuating light conditions, potentially promoting plant growth (Kromdijk et al., 2016). The greater increase of NPQ kinetics in cold vs drought treated plants suggests temperature-depended changes in the activity of both NPQ-related enzymes, violaxanthin de-epoxidase (VDE) and zeaxanthin epoxidase (ZEP) (Nilkens et al., 2010).

Results in our detailed photosynthesis study aligned with the globally observed association of later flowering with higher $\delta^{13}C$. For example, Baa-1 from lowland northern Europe had the latest flowering and showed the highest intrinsic water use efficiency at higher light intensities (Table S8). Our gas exchange data also aligned with the central Asian association of earlier flowering with higher survival rates under high light. The early flowering Dja-1 had significantly higher NPQ at higher light intensities than the later flowering Sij-1. This suggests that in Dja-1 NPQ mechanisms are critical against high light stress. Surprisingly, the only significant difference in NPQ kinetics between these two ecotypes was during NPQ relaxation, which was lower in Dja-1 under control and stress conditions. The significantly lower NPQ at all light levels in Sij-1 is most likely due to high photochemical quenching and can be a result of lower expression of PsbS which in turn might contribute to the observed higher stomatal conductance by affecting a chloroplast-derived signal for stomatal opening in response to light (Glowacka et al., 2018).

Conclusions

Genomic and eco-physiologic elevational clines in Arabidopsis represent diverse strategies that respond to different stressful conditions along elevation in different regions. We found that these strategies are mediated by a complex relationship between seasonal timing and homeostatic regulation in response to stress and are potentially underlined by different genomic variants and genes in different regions (see (Lopez-Arboleda et al., 2021). Thus, every mountain range might have a specific adaptive cline. Our regional approach highlights how different mountains can idiosyncratically affect the genomic and phenotypic diversity of plants.

Methods

Plant material for diversity panel

A diverse set of 233 ecotypes (i.e., natural genotypes), the collection of which we refer to as a diversity panel (Table S1), were selected from the 1001 genomes panel of resequenced natural

inbred lines obtained from ABRC (Alonso-Blanco et al., 2016) in addition to 20 Moroccan ecotypes obtained from NASC (Brennan et al., 2014, Durvasula et al., 2017). We specifically targeted several regional elevational gradients with this diversity panel. Additionally, we collected 17 new lines from the field along elevational gradients in Uganda (in 2018) and Ethiopia (in 2017), ranging from 3691–4374 m. We classified our diversity panel into four regions: central Asia (also including Lebanon, the Caucasus and the Urals, N=76), western Mediterranean (i.e., Iberia and Morocco, N=112), eastern Africa (i.e., Ethiopia, Uganda and Tanzania, N=18), and Europe (excluding Iberia and Russia; N=55). The remaining accessions were from North America and Japan, thus designated as introduced (N=8), and one accession from Cape Verde was left as unassigned given how different this location is from all other regions.

With this diversity panel we conducted three large-scale growth chamber experiments focused on traits related to resource use and oxidative stress (Experiment 1–3, see Supplemental Methods 1 for details on planting conditions and protocols). We grew 116–253 ecotypes from 3–4 regions under high elevation conditions, to investigate stress due to low pCO_2, high light and night-time freezing. We also performed a detailed study on photosynthetic recovery after cold based on 12 ecotypes with a global distribution (Table S1).

Experiment 1: Low pCO_2 conditions with 253 ecotypes

We imposed a treatment of low pCO_2 by scrubbing CO_2 from the growth chamber air using a soda lime absorbent material (SODASORB HP, Divers Supply Inc., Gretna, LA). We set the growth chamber to 200 ppm CO_2, which at our elevation of ~350 m corresponds to ~19.5 Pa, the approximate pre-industrial partial pressure of CO_2 at 3000 m, compared to a pre-industrial partial pressure of ~28 Pa at sea level. We sought to mimic high elevation conditions by growing plants in high light and cool conditions (Table S3). We randomly selected 144 ecotypes for 5 replicates and 114 ecotypes for only 4 replicates due to space constraints. To limit positional effects, we periodically rotated trays in three positions clockwise and front to back, and to a different randomly selected location within the growth chamber.

We recorded phenotypic variation in nine morphological and resource use traits: leaf temperature, root diameter, rosette diameter and compactness, $\delta^{13}C$, $\delta^{15}N$, C: N, stomatal density, and length.

We recorded leaf temperature 109 days after planting and just after setting temperature to 5–6° C in the growth chamber. Thermal images were taken with a FLIR ONE (Gen 2) thermal camera for iOS (FLIR Systems, USA) on one mid-aged representative leaf per replicate after removing trays from the growth chamber.

We terminated the experiment 156 days after planting and subsequently completed harvesting and phenotyping within five days. We took rosette diameter and compactness with ImageJ (Schneider et al. 2012) from overhead photographs of plants just prior to harvest. For rosette diameter, we used the average between the longest and the shortest distance between opposite leaf tips. For rosette compactness we assigned a rating from 1–5 where 5 corresponded to more compact rosettes with shorter petioles and total leaf overlap, thus less soil exposure and 1 corresponded to less compact rosettes with longer petioles and minimal leaf overlap, thus more soil exposure. Root diameter was measured 3 mm below the hypocotyl/root junction using a caliper.

We used 2–4 young healthy leaves per plant for estimating $\delta^{13}C$, $\delta^{15}N$, and total carbon and nitrogen composition. Leaves of each ecotype were pooled, dried at 27°C for 24 h in

envelopes, ground to a fine powder and homogenized using a mortar and pestle. We packaged a 1.5 – 2.5 mg aliquot of finely ground leaf tissue from each rosette into an 8 x 5 mm tin capsule (EA Consumables, Pennsauken, NJ). Samples were sent to the University of California Davis Stable Isotope Facility for $\delta^{13}C$, $\delta^{15}N$, and total carbon and nitrogen composition was analyzed using an elemental analyzer interfaced to a continuous flow isotope ratio mass spectrometer (IRMS).

We measured stomatal density and length on a smaller dataset; 2–4 young healthy leaves were collected per ecotype and stored in 75% ethanol at 4°C. We took epidermal peels from the abaxial surface of each leaf after softening leaves by soaking in distilled water for 3–7 minutes. Epidermal peels were immediately placed into 0.02% Toluidine Blue stain for 3–5 minutes, rinsed with DI water for 3 seconds and put onto a slide with a small drop of DI water for imaging. Images were taken at 20X magnification using a Zeiss compound microscope. We estimated stomatal density (stomata/mm^2) and measured guard cell length (mm) with ImageJ, using distance-calibrated images of one representative area of the epidermal peel where we measured the length ten stomata.

Experiment 2 and 3: Contrasting light and night-time temperature with 114–172 ecotypes

We conducted Experiment 2 using identical growth parameters except for light intensity (Table S4). Five replicates of the same 114 ecotypes were grown under two light levels under cool conditions. Plants grown on the lower level of the growth chamber received the "high light" treatment with 100% maximum light output (~616 PAR), and plants grown on the upper level of the chamber received the "low light" treatment with 57% maximum light output (~350 PAR). We recorded soil temperature 43 days after planting using a FLIR ONE (Gen 2) thermal camera. As expected, soils were warmer in pots under the high light treatment, with a mean and median temperature of 12.4 and 12.6°C respectively under high light, and a mean and median temperature of 11.1 and 11.2°C respectively under low light.

We then conducted Experiment 3, consisting of two separate consecutive experiments using identical growth parameters except for night-time temperatures (Table S5). Six replicates of the same 172 ecotypes were grown under night-time below freezing temperature and consecutively under night-time above freezing temperature. Both experiments maintained similar high light, cool conditions during the day and we used six pots of Col-0 containing 5TE probes (METER Group, Inc., Pullman WA, USA) to monitor soil temperature every 30 minutes.

In both Experiments 2 and 3, we rotated trays periodically and recorded phenotypic variation in three traits related to photosynthesis: fresh aboveground mass, antioxidant activity, and pigmentation. Ecotypes were harvested 82–89 days (Experiment 2) and 72–75 days (Experiment 3) after planting. All replications from a randomly selected ecotype were harvested and pooled together at a time for assessing collective fresh aboveground mass and antioxidant activity with 1,1-diphenyl-2-picrylhydrazyl (DPPH), an assay that estimates free radical scavenging activity of antioxidants (see Supplemental Methods 2 for a detailed protocol). Pigmentation was estimated with ImageJ, and late germinants were not analyzed for color. In Experiment 2, rosette leaf color was measured from the pixels selected at a representative location within a mid-aged leaf on photographs taken just prior to harvest. We used the option "Color Histogram" to obtain the variation and calculate percent of RGB values. In Experiment 3, we obtained variation in RGB values from images of the plant extracts in test tubes used for DPPH. Images were white balanced and zoomed into the test tube avoiding any discolored, dark, or bright areas. We note that upon visual examination of photographs rosette colors are probably

more indicative of anthocyanins, while extract colors may also inform on other pigments like carotenoids, including xanthophylls.

Assessing regional-specific environmental and phenotypic elevational-clines

After evaluating the accuracy of coordinates and elevation of ecotypes, we first examined the regional variation of environmental variables on elevation using linear models with the 'lm' function in R. To understand how study regions varied climatically we performed a principal component analysis (PCA) on 85 environmental variables (Table S2).

We obtained breeding values of measured phenotypes from the fixed effects of a linear mixed model that estimated the trait mean of each ecotype while accounting for the experimental tray where replicates were located as a random factor. We summarized variation in phenotypes from Experiment 1 and days to flower (in plants grown at 10 and 16 ºC) with a PCA (PC_{Exp1}). We performed the same analysis to summarize variation in color space assessed from RGB values in the two contrasting conditions of both Experiment 2 and 3: $PC_{LeavesColor}$ and $PC_{ExtractsColor}$, respectively. Based on the color space in PC1 and PC2, we calculated plasticity in color based on the Euclidean distance between values of the two contrasting conditions of same ecotype in each experiment using the Pythagorean theorem. We also calculated plasticity in antioxidant activity by finding the difference between experimental conditions. Survival per ecotype in Experiment 2 and 3 were obtained from the number of replicates that survived at the end of each experiment divided by the number of replicates that germinated within treatments. We used survival as a proxy of fitness and analyzed how other traits affect it.

We used ANOVA to test for differences in trait variation among regions, followed by Tukey's honest significant difference post-hoc tests to find pairwise regional differences. We also used ANOVA to test for phenotypic plasticity between experimental conditions in Experiment 2 and 3, i.e., significant differences in trait variation between conditions.

For each trait of interest, including the first two PCs of Experiment 1–3 described above; PC_{Exp1}, $PC_{LeavesColor}$ and $PC_{ExtractsColor}$, we tested for regional associations with elevation and selected climate variables, including variables related with the growing seasons (length, aridity index and minimum temperature), and isothermality (i.e., day to year variation in temperature). We subsetted by regions: central Asia, western Mediterranean, Europe and eastern Africa, and used linear models (lm in R) with elevation as the explanatory variable within each region. To account for multiple testing, we used a false discovery rate (FDR) threshold of 0.05 across p-values for each region (i.e., datasets). For traits where we found significant relationships based on FDR, we subsequently performed linear-mixed effects kinship models, with 'lmekin' in R (Therneau, 2012), which accounted for population genetic structure by incorporating a kinship matrix of ecotypes as a random effect. We used results from the latter models to estimate if trait variation is mediated by selection along elevational clines. We used ggplot2 to plot linear regressions (Wickham et al., 2016).

Assessing genome-wide phenotypic associations and genomic clines

We used ecotypes that had been previously resequenced (Alonso-Blanco et al., 2016, Durvasula et al., 2017), and included eight eastern African ecotypes that were newly resequenced for this study (Supplemental Methods 3). A final imputed VCF contained 1225 accessions of which up to 261 were in our study, and 22'619,232 SNPs of which 11'500,298 were polymorphic (Supplemental Methods 3). To visualize population genetic structure, we constructed a neighbor-joining tree with a subset of 205,667 unlinked SNPs obtained in SNPRelate with an LD threshold

of 0.2 and a 10 kb window. With this set of SNPs, we calculated a distance matrix based on genetic dissimilarity between ecotypes and used the 'nj' and 'plotnj' function in the R package ape (Paradis et al., 2004).

We used univariate linear mixed-effects models in GEMMA (v 0.98.3) to perform genome wide association studies (GWAS). Because traits generally differed in the number of analyzed individuals, we filtered loci with <0.05 MAF directly in GEMMA. To account for multiple testing, we used an FDR threshold of 0.05 to detect significantly associated SNPs with traits of interest. We ran GEMMA on the global dataset for all traits, as well as by region for those traits that showed a significant association with elevation (FDR<0.05): flowering time, $\delta^{13}C$, and fresh aboveground mass under high and low light in the western Mediterranean, and flowering time in central Asia. For flowering time, we used all the ecotypes with available data: 192 for western Mediterranean and 109 for central Asia. We identified QTL by assigning the top SNPs (i.e., those with the lowest 25 p-values for each trait) to candidate genes using the Araport11 reannotation (Cheng et al., 2017) and a 5 kb window. For top SNPs in putative QTLs, we evaluated the association of allelic variation with elevation while accounting for population genetic structure in GEMMA to evaluate if selection on elevation maintains allelic variation.

Assessing photosynthetic capacity and NPQ kinetics in a focused physiology panel

To characterize photosynthetic capacity and NPQ dynamics along elevation, we selected a subset of 11 ecotypes (Table S1), representing a global set from 22–4078 m (see Supplemental Methods 4 for growing conditions).

NPQ kinetics— Two weeks after germination (i.e., at the seedling stage) NPQ was measured in two separate experiments using a fluorescence imager (Closed FluorCam FC 800-C, Photon Systems Instruments, Drasov, Czech Republic). Seedlings were subjected to drought (5 days of withholding the watering) or to 17 hours of overnight chilling of 4°C. Half of the seedlings in each experiment where not submitted to cold or drought to serve as a corresponding control. Seedlings were grown in 9 x 12 potting trays (809 series, Hummert International). Plant material was first dark adapted for 20 min at room temperature after which the dark-adapted minimum fluorescence (F_o) and maximal fluorescence (F_m) were imaged using an 800 ms pulse of saturating light (2400 µmol m^{-2} s^{-1}, cool white 6500 K). Subsequently, plants were subjected to three cycles of 3 min 1000 µmol m^{-2} s^{-1} (combination of 500 µmol m^{-2} s^{-1}; λ_{max} = 617 nm and 500 µmol m^{-2} s^{-1} cool white 6500 K) followed by 2 min of dark. NPQ of chlorophyll fluorescence was determined assuming the Stern-Volmer quenching model (NPQ = F_m/F_m' - 1; Bilger and Bjorkman, 1994). To calculate the NPQ according to the saturating flashes were provided to image variable fluorescence (F') and the maximum fluorescence under illuminated conditions (F_m') at following intervals 10s, 10s, 20s, 20s, 60s and 60s in light and 10s, 20s, 30s and 60s in dark.

Raw images were processed manually using FluorCam 7 software (Photon Systems Instruments) by drawing three circles per plant of 170–180 pixels on three young fully developed leaves. The NPQ data were fitted to exponential equations to parametrize the NPQ kinetics of its induction in light and relaxation in dark of three subsequent light-dark cycles (Fig. S7) using a custom-made script in MATLAB (MATLAB R2018b, MathWorks, Natick, MA, USA). Baa-1 and JL-011-2-1 were not present in the drought experiment due to low germination.

Gas exchange— Thirty days after germination (i.e., at the pre-flowering stage), we measured gas exchange using an open gas exchange system LI-6800 (LI-COR, Inc. Lincoln, NE, USA) equipped with a 2 cm^2 leaf cuvette chamber and an integrated modulated fluorometer

(6800-01A, LI-COR). We selected the youngest fully expanded leaves large enough to fill the leaf cuvette for measurements. Block temperature was maintained at 23°C, [CO_2] inside the cuvette at 400 µmol mol^{-1}, and leaf-to-air water vapor pressure deficit between 1.1 and 1.2 kPa. To determine the light response of net assimilation (A_n), non-photochemical quenching (NPQ), and whole-chain photosynthetic electron transport (J), we measured the gas exchange and pulse amplitude-modulated chlorophyll fluorescence at a range of light intensities. All fluorescence parameters were recorded using a multiphase flash routine (Loriaux et al., 2013). Leaves were dark-adapted overnight and in the leaf cuvette for an additional 20 minutes, after which minimal (F_o) and maximal fluorescence (F_m) were measured to determine maximal efficiency of whole-chain electron transport ($F_v/F_m = (F_m - F_o)/ F_m$) (Genty et al., 1989). We subsequently slowly increased light intensity (90% red LEDs λ_{peak} 630 nm and 10% blue λ_{peak} 460 nm) from 0 to 50, 80, 110, 140, 170, 200, 300, 400, 500, 700, 800, 1000 µmol m^{-2} s^{-1}. When steady state was reached, A_n, stomatal conductance (g_s), and intercellular CO_2 concertation (C_i) were logged, and variable fluorescence (F') and F_m' were measured to estimate the operating efficiency of photosystem II (Φ_{PSII}; $\Phi_{PSII} = (F_m' - F')/ F_m'$; Genty et al., 1989). Minimal fluorescence without dark adaptation (F_o') was also determined (using a short far-red pulse to fully oxidize Q_A). Quantum efficiency of linear electron transport ($\Phi_{PSIImax}$) and quantum efficiency of leaf net CO_2 assimilation (Φ_{CO2max}) were derived from the initial slope of the light response of J and A_n, respectively. Mitochondrial respiration rate in the light (R_d) and A_{sat} were obtained by fitting the light response curves of A_n to a nonrectangular hyperbola equation (Long, 2003), similarly J_{max} was derived from the asymptote of the nonrectangular hyperbola fitted to the light responses of J.

In addition to the steady state light response curves, a dynamic light response curve was reconstructed from a time series of changes in light intensity. First, leaves were allowed to reach steady state gas exchange at 1000 µmol m^{-2} s^{-1}. Subsequently, light intensity was changed from 1000 to 800, 700, 400, 300, 200, 170, 140, 110, 80 and 50 µmol m^{-2} s^{-1}, where each step lasted 4 min and was preceded by 4 min of 1000 µmol m^{-2} s^{-1}. At each light intensity, F', F_m' and gas exchange parameters were determined after 60s, 140s and 220s. The values of these three measurements were averaged and used to reconstruct light response curves under fluctuating light. The dynamic light response curves were taken on the same plants as steady state response curves. The resulting data were analyzed as described above. Three ecotypes (Ara-1, IP-Trs-0, and NFA-10) were not included due to early flowering.

Quantification of photosynthesis-related pigments— 2.32 cm^2 leaf tissue were collected from the interveinal region, snap-frozen in liquid nitrogen and stored at –80°C until further processing. Tissue was ground in liquid nitrogen under dim light. 600 µl of pre-cooled 100% methanol (A452-1, Fisher Scientific, Hampton, NH, USA) was added to the ground tissue and vortexed. The samples were incubated on ice for 4 hours with additional vortexing at 30, 60, and 180 min. After 4 h, tubes were centrifuged for 5 min at 4500 rpm in the pre-cooled centrifuge. The supernatant was transferred to a fresh tube and an additional 400 µl of methanol was added to the pellet to extract any residual pigments, these steps were repeated until the pellet became completely white. The supernatant was transferred to 96 well plates and absorption at 470, 652, 665 nm was measured using a plate reader (Synergy™ 2, BioTek® Instruments, Inc, Winooski, VT, USA) with Gen5 software. Concentrations of chlorophyll *a*, *b* and total carotenoids were determined from absorption using the methanol-based coefficients by Lichtenthaler (1987).

Estimation of growth— The above ground fraction of 30-day plants for 11 ecotypes was harvested and immediately weighted to estimate fresh weight. To estimate dry weight, fresh weights were dried to constant weight at 70°C.

Statistical analysis— Statistical analyses were performed with SAS (version 9.4, SAS Institute Inc., Cary, NC, USA). Data were tested with the Brown–Forsythe test for homogeneity of variance and the Shapiro–Wilk test for normality. If either test discarded the null hypothesis, data were transformed, or a Wilcoxon non-parametric test was applied followed by a Kruskal-Wallis test. One-way analysis of variance was applied to gas exchange and fluorescence data, photosynthesis-related pigments, and biomass.

Accession numbers

Sequence data from this article will be found in the GenBank data library.

Acknowledgments

Permits: Plant material was exported from Uganda with permission of The Ministry of Agriculture, Animal Industry and Fisheries' Plant Quarantine and Inspection Services, permit UQIS 4414/93/PC (E). Material was exported from Ethiopia with permission of the Ethiopian Biodiversity Institute, Ref. no. EBE71/7065/2018. Material was imported to the USA under USDA APHIS permits P37-17-01651 and P37-18-00230. We thank Chloee McLaughlin, Jeremy Sutherland, Tim Gilpatrick, Connor Campana, Victoria Meagher, and Jaden Hill for assistance in experiment setup and rosette harvests. We thank Shawn Berghard for assistance and advice in pest and disease control. Funding was provided by NSF DEB-1927009 and NIH 1R35GM138300-01 awards to JRL.

Author contributions

DG, CL, SS, KG, and JRL designed the research; DG, CL, AH, SS, LL, TX, EK, DE, JK, MY, CEB, and TW performed research; DG, CL, SS, LL, TX, EK analyzed data; DG, CL, SS, KG, and JRL wrote the paper with contributions of all other authors.

References

Ågren, J. and Schemske, D.W. (2012). Reciprocal transplants demonstrate strong adaptive differentiation of the model organism *Arabidopsis thaliana* in its native range. New Phytologist **194**: 1112–1122.

Alonso-Blanco, C. et al. (2016). 1,135 Genomes Reveal the Global Pattern of Polymorphism in *Arabidopsis thaliana*. Cell **166**: 481–491.

Anderson, J.T., Wagner, M.R., Rushworth, C.A., Prasad, K.V.S.K., and Mitchell-Olds, T. (2014). The evolution of quantitative traits in complex environments. Heredity **112**: 4–12.

Bilger, W. and Bjorkman, O. (1994). Relationships among violaxanthin deepoxidation, thylakoid membrane conformation, and nonphotochemical chlorophyll fluorescence quenching in leaves of cotton (Gossypium hirsutum L.). Planta **193**.

Bohutínská, M., Vlček, J., Yair, S., Laenen, B., Konečná, V., Fracassetti, M., Slotte, T., and Kolář, F. (2021). Genomic basis of parallel adaptation varies with divergence in *Arabidopsis* and its relatives. Proc Natl Acad Sci USA **118**: e2022713118.

Brennan, A.C., Méndez-Vigo, B., Haddioui, A., Martínez-Zapater, J.M., Picó, F.X., and Alonso-Blanco, C. (2014). The genetic structure of Arabidopsis thaliana in the south-western Mediterranean range reveals a shared history between North Africa and southern Europe. BMC Plant Biol **14**: 17.

Brochmann, C., Gizaw, A., Chala, D., Kandziora, M., Eilu, G., Popp, M., Pirie, M.D., and Gehrke, B. (2021). History and evolution of the afroalpine flora: in the footsteps of Olov Hedberg. Alpine Botany.

Caldas, F.J. (1966). Obras completas de Francisco José de Caldas: publicadas por la Universidad Nacional de Colombia como homenaje con motivo del sesquicentenario de su muerte 1816 - Octubre 29 - 1966 (Imprenta Nacional: Bogotá, Colombia).

Cheng, C.-Y., Krishnakumar, V., Chan, A.P., Thibaud-Nissen, F., Schobel, S., and Town, C.D. (2017). Araport11: a complete reannotation of the Arabidopsis thaliana reference genome. The Plant Journal **89**: 789–804.

Clausen, J., Keck, D.D., and Hiesey, W.M. (1940). Experimental studies on the nature of species. I. Effect of varied environments on western North American plants. Experimental studies on the nature of species. I. Effect of varied environments on western North American plants.

DeLeo, V.L., Menge, D.N.L., Hanks, E.M., Juenger, T.E., and Lasky, J.R. (2020). Effects of two centuries of global environmental variation on phenology and physiology of *Arabidopsis thaliana*. Glob Change Biol **26**: 523–538.

Demmig-Adams, B. (1990). Carotenoids and photoprotection in plants: A role for the xanthophyll zeaxanthin. Biochimica et Biophysica Acta (BBA) - Bioenergetics **1020**: 1–24.

Deng, W., Ying, H., Helliwell, C.A., Taylor, J.M., Peacock, W.J., and Dennis, E.S. (2011). *FLOWERING LOCUS C* (*FLC*) regulates development pathways throughout the life cycle of Arabidopsis. Proc Natl Acad Sci USA **108**: 6680–6685.

Des Marais, D.L., Auchincloss, L.C., Sukamtoh, E., McKay, J.K., Logan, T., Richards, J.H., and Juenger, T.E. (2014). Variation in MPK12 affects water use efficiency in Arabidopsis and reveals a pleiotropic link between guard cell size and ABA response. Proc Natl Acad Sci USA **111**: 2836–2841.

Distelbarth, H., Nägele, T., and Heyer, A.G. (2013). Responses of antioxidant enzymes to cold and high light are not correlated to freezing tolerance in natural accessions of *Arabidopsis thaliana*. Plant Biol J **15**: 982–990.

Dittberner, H., Korte, A., Mettler-Altmann, T., Weber, A.P.M., Monroe, G., and de Meaux, J. (2018). Natural variation in stomata size contributes to the local adaptation of water-use efficiency in *Arabidopsis thaliana*. Mol Ecol **27**: 4052–4065.

Durvasula, A., Fulgione, A., Gutaker, R.M., Alacakaptan, S.I., Flood, P.J., Neto, C., Tsuchimatsu, T., Burbano, H.A., Picó, F.X., Alonso-Blanco, C., and Hancock, A.M. (2017). African genomes illuminate the early history and transition to selfing in *Arabidopsis thaliana*. Proc Natl Acad Sci USA **114**: 5213–5218.

Exposito-Alonso, M. (2020). Seasonal timing adaptation across the geographic range of *Arabidopsis thaliana*. Proc Natl Acad Sci USA **117**: 9665–9667.

Fernández-Marín, B., Gulías, J., Figueroa, C.M., Iñiguez, C., Clemente-Moreno, M.J., Nunes-Nesi, A., Fernie, A.R., Cavieres, L.A., Bravo, L.A., García-Plazaola, J.I., and Gago, J. (2020). How do vascular plants perform photosynthesis in extreme environments? An integrative ecophysiological and biochemical story. Plant J **101**: 979–1000.

Fournier-Level, A., Korte, A., Cooper, M.D., Nordborg, M., Schmitt, J., and Wilczek, A.M. (2011). A Map of Local Adaptation in *Arabidopsis thaliana*. Science **334**: 86–89.

Frachon, L., Bartoli, C., Carrère, S., Bouchez, O., Chaubet, A., Gautier, M., Roby, D., and Roux, F. (2018). A Genomic Map of Climate Adaptation in Arabidopsis thaliana at a Micro-Geographic Scale. Front. Plant Sci. **9**: 967.

Fulgione, A. and Hancock, A.M. (2018). Archaic lineages broaden our view on the history of *Arabidopsis thaliana*. New Phytol **219**: 1194–1198.

García-Plazaola, J.I., Esteban, R., Fernández-Marín, B., Kranner, I., and Porcar-Castell, A. (2012). Thermal energy dissipation and xanthophyll cycles beyond the Arabidopsis model. Photosynthesis Research **113**: 89–103.

Genty, B., Briantais, J.-M., and Baker, N.R. (1989). The relationship between the quantum yield of photosynthetic electron transport and quenching of chlorophyll fluorescence. Biochimica et Biophysica Acta (BBA) - General Subjects **990**: 87–92.

Glowacka, K., Kromdijk, J., Kucera, K., Xie, J., Cavanagh, A.P., Leonelli, L., Leakey, A.D.B., Ort, D.R., Niyogi, K.K., and Long, S.P. (2018). Photosystem II Subunit S overexpression increases the efficiency of water use in a field-grown crop. Nature Communications **9**: 868.

Gorsuch, P. A., Pandey, S., and Atkin, O. K. (2010). Thermal de-acclimation: how permanent are leaf phenotypes when cold-acclimated plants experience warming? Plant, Cell & Environment **33**: 1124–1137.

Graeber, K. et al. (2014). *DELAY OF GERMINATION 1* mediates a conserved coat-dormancy mechanism for the temperature- and gibberellin-dependent control of seed germination. Proc Natl Acad Sci USA **111**: E3571–E3580.

Günther, T., Lampei, C., Barilar, I., and Schmid, K.J. (2016). Genomic and phenotypic differentiation of *Arabidopsis thaliana* along altitudinal gradients in the North Italian Alps. Mol Ecol **25**: 3574–3592.

Hannah, M.A., Wiese, D., Freund, S., Fiehn, O., Heyer, A.G., and Hincha, D.K. (2006). Natural Genetic Variation of Freezing Tolerance in Arabidopsis. Plant Physiology **142**: 98–112.

Havaux, M., Dall'Osto, L., and Bassi, R. (2007). Zeaxanthin Has Enhanced Antioxidant Capacity with Respect to All Other Xanthophylls in Arabidopsis Leaves and Functions Independent of Binding to PSII Antennae. Plant Physiology **145**: 1506–1520.

Havaux, M. and Kloppstech, K. (2001). The protective functions of carotenoid and flavonoid pigments against excess visible radiation at chilling temperature investigated in Arabidopsis npq and tt mutants. Planta **213**: 953–966.

Hepworth, J. et al. (2020). Natural variation in autumn expression is the major adaptive determinant distinguishing Arabidopsis *FLC* haplotypes. eLife **9**: e57671.

Hetherington, S.E., He, J., and Smillie, R.M. (1989). Photoinhibition at Low Temperature in Chilling-Sensitive and -Resistant Plants. Plant Physiol. **90**: 1609–1615.

Huo, H., Wei, S., and Bradford, K.J. (2016). *DELAY OF GERMINATION1* (*DOG1*) regulates both seed dormancy and flowering time through microRNA pathways. Proc Natl Acad Sci USA **113**: E2199–E2206.

Jeong, J., Cohu, C., Kerkeb, L., Pilon, M., Connolly, E.L., and Guerinot, M.L. (2008). Chloroplast Fe (III) chelate reductase activity is essential for seedling viability under iron limiting conditions. Proceedings of the National Academy of Sciences **105**: 10619–10624.

Jeong, J. and Connolly, E.L. (2009). Iron uptake mechanisms in plants: Functions of the FRO family of ferric reductases. Plant Science **176**: 709–714.

Juszczak, I., Cvetkovic, J., Zuther, E., Hincha, D.K., and Baier, M. (2016). Natural Variation of Cold Deacclimation Correlates with Variation of Cold-Acclimation of the Plastid Antioxidant System in *Arabidopsis thaliana* Accessions. Front. Plant Sci. **7**.

Kenney, A.M., McKay, J.K., Richards, J.H., and Juenger, T.E. (2014). Direct and indirect selection on flowering time, water-use efficiency (WUE, $\delta^{13}C$), and WUE plasticity to drought in *Arabidopsis thaliana*. Ecol Evol **4**: 4505–4521.

Kim, J.-S., Lim, J.Y., Shin, H., Kim, B.-G., Yoo, S.-D., Kim, W.T., and Huh, J.H. (2019). ROS1-Dependent DNA Demethylation Is Required for ABA-Inducible *NIC3* Expression. Plant Physiol. **179**: 1810–1821.

Kooyers, N.J., Greenlee, A.B., Colicchio, J.M., Oh, M., and Blackman, B.K. (2015). Replicate altitudinal clines reveal that evolutionary flexibility underlies adaptation to drought stress in annual *Mimulus guttatus*. New Phytol **206**: 152–165.

Körner, C. (2021). Alpine Plant Life: Functional Plant Ecology of High Mountain Ecosystems (Springer International Publishing: Cham).

Körner, C. (2003). Ecological impacts of atmospheric CO_2 enrichment on terrestrial ecosystems. Philosophical Transactions of the Royal Society of London. Series A: Mathematical, Physical and Engineering Sciences **361**: 2023–2041.

Körner, C. (2007). The use of 'altitude'in ecological research. Trends in ecology & evolution **22**: 569–574.

Kromdijk, J., Głowacka, K., Leonelli, L., Gabilly, S.T., Iwai, M., Niyogi, K.K., and Long, S.P. (2016). Improving photosynthesis and crop productivity by accelerating recovery from photoprotection. Science **354**: 857–861.

Lampei, C., Wunder, J., Wilhalm, T., and Schmid, K.J. (2019). Microclimate predicts frost hardiness of alpine *Arabidopsis thaliana* populations better than elevation. Ecol Evol **9**: 13017–13029.

Li, P., Filiault, D., Box, M.S., Kerdaffrec, E., van Oosterhout, C., Wilczek, A.M., Schmitt, J., McMullan, M., Bergelson, J., and Nordborg, M. (2014). Multiple FLC haplotypes defined by independent cis-regulatory variation underpin life history diversity in Arabidopsis thaliana. Genes & Development **28**: 1635–1640.

Li, P., Li, Y.-J., Zhang, F.-J., Zhang, G.-Z., Jiang, X.-Y., Yu, H.-M., and Hou, B.-K. (2017). The Arabidopsis UDP-glycosyltransferases UGT79B2 and UGT79B3, contribute to cold, salt and drought stress tolerance via modulating anthocyanin accumulation. Plant J **89**: 85–103.

Lichtenthaler, H.K. (1987). [34] Chlorophylls and carotenoids: Pigments of photosynthetic biomembranes. In Methods in Enzymology (Academic Press), pp. 350–382.

Long, S.P. (2003). Gas exchange measurements, what can they tell us about the underlying limitations to photosynthesis? Procedures and sources of error. Journal of Experimental Botany **54**: 2393–2401.

Lopez-Arboleda, W.A., Reinert, S., and Nordborg, M. (2021). Global genetic heterogeneity in adaptive traits. Molecular Biology and Evolution **38**: 4822–4831.

Loriaux, J.M., Lenderink, G., De Roode, S.R., and Siebesma, A.P. (2013). Understanding Convective Extreme Precipitation Scaling Using Observations and an Entraining Plume Model. Journal of the Atmospheric Sciences **70**: 3641–3655.

Lovell, J.T., Juenger, T.E., Michaels, S.D., Lasky, J.R., Platt, A., Richards, J.H., Yu, X., Easlon, H.M., Sen, S., and McKay, J.K. (2013). Pleiotropy of *FRIGIDA* enhances the potential for multivariate adaptation. Proc. R. Soc. B. **280**: 20131043.

Ludlow, M.M. (1989). Strategies of response to water stress. In Structural and Functional Responses to Environmental Stresses, K.H. Kreeb, H. Richter, and T.M. Hinckley, eds (SPB Academic), pp. 269–281.

Luo, Y., Dong, X., Yu, T., Shi, X., Li, Z., Yang, W., Widmer, A., and Karrenberg, S. (2015a). A Single Nucleotide Deletion in *Gibberellin20-oxidase1* Causes Alpine Dwarfism in Arabidopsis. Plant Physiol. **168**: 930–937.

Luo, Y., Widmer, A., and Karrenberg, S. (2015b). The roles of genetic drift and natural selection in quantitative trait divergence along an altitudinal gradient in Arabidopsis thaliana. Heredity **114**: 220–228.

Malnoë, A. (2018). Photoinhibition or photoprotection of photosynthesis? Update on the (newly termed) sustained quenching component qH. Environmental and Experimental Botany **154**: 123–133.

Martínez-Berdeja, A., Stitzer, M.C., Taylor, M.A., Okada, M., Ezcurra, E., Runcie, D.E., and Schmitt, J. (2020). Functional variants of *DOG1* control seed chilling responses and variation in seasonal life-history strategies in *Arabidopsis thaliana*. Proc Natl Acad Sci USA **117**: 2526–2534.

Mckay, J.K., Richards, J.H., and Mitchell-Olds, T. (2003). Genetics of drought adaptation in *Arabidopsis thaliana*: I. Pleiotropy contributes to genetic correlations among ecological traits. Molecular Ecology **12**: 1137–1151.

Méndez-Vigo, B., Picó, F.X., Ramiro, M., Martínez-Zapater, J.M., and Alonso-Blanco, C. (2011). Altitudinal and Climatic Adaptation Is Mediated by Flowering Traits and *FRI*, *FLC*, and *PHYC* Genes in Arabidopsis. Plant Physiology **157**: 1942–1955.

Méndez-Vigo, B., Savic, M., Ausín, I., Ramiro, M., Martín, B., Picó, F.X., and Alonso-Blanco, C. (2016). Environmental and genetic interactions reveal *FLOWERING LOCUS C* as a modulator of the natural variation for the plasticity of flowering in Arabidopsis: Genetic mechanisms of the plasticity of flowering. Plant Cell Environ **39**: 282–294.

Miyaji, T., Kuromori, T., Takeuchi, Y., Yamaji, N., Yokosho, K., Shimazawa, A., Sugimoto, E., Omote, H., Ma, J.F., Shinozaki, K., and Moriyama, Y. (2015). AtPHT4;4 is a chloroplast-localized ascorbate transporter in Arabidopsis. Nat Commun **6**: 5928.

Montesinos, A., Tonsor, S.J., Alonso-Blanco, C., and Picó, F.X. (2009). Demographic and Genetic Patterns of Variation among Populations of Arabidopsis thaliana from Contrasting Native Environments. PLoS ONE **4**: e7213.

Montesinos-Navarro, A., Picó, F.X., and Tonsor, S.J. (2012). Clinal Variation in Seed Traits Influencing Life Cycle Timing In *Arabidopsis thaliana*. Evolution **66**: 3417–3431.

Montesinos-Navarro, A., Wig, J., Xavier Pico, F., and Tonsor, S.J. (2011). *Arabidopsis thaliana* populations show clinal variation in a climatic gradient associated with altitude. New Phytologist **189**: 282–294.

Muller, P., Li, X.-P., and Niyogi, K.K. (2001). Non-photochemical quenching. A response to excess light energy. Plant physiology **125**: 1558–1566.

Nakabayashi, R. et al. (2014). Enhancement of oxidative and drought tolerance in Arabidopsis by overaccumulation of antioxidant flavonoids. Plant J **77**: 367–379.

Nilkens, M., Kress, E., Lambrev, P., Miloslavina, Y., Müller, M., Holzwarth, A.R., and Jahns, P. (2010). Identification of a slowly inducible zeaxanthin-dependent component of non- photochemical quenching of chlorophyll fluorescence generated under steady-

state conditions in Arabidopsis. Biochimica Et Biophysica Acta (BBA) Bioenergetics **1797**: 466–475.

Niyogi, K. K., Grossman, A. R., and Bjorkman, O. (1998). Arabidopsis mutants define a central role for the xanthophyll cycle in the regulation of photosynthetic energy conversion. Plant Cell **10**: 1121–1134.

Paradis, E., Claude, J., and Strimmer, K. (2004). APE: analyses of phylogenetics and evolution in R language. Bioinformatics **20**: 289–290.

Picó, F.X. (2012). Demographic fate of *Arabidopsis thaliana* cohorts of autumn- and spring-germinated plants along an altitudinal gradient: Cohort dynamics of *Arabidopsis thaliana*. Journal of Ecology **100**: 1009–1018.

Rungrat, T., Almonte, A.A., Cheng, R., Gollan, P.J., Stuart, T., Aro, E., Borevitz, J.O., Pogson, B., and Wilson, P.B. (2019). A Genome-Wide Association Study of Non-Photochemical Quenching in response to local seasonal climates in *Arabidopsis thaliana*. Plant Direct **3**.

Sánchez-Bermejo, E., Méndez-Vigo, B., Pico, F.X., Martínez-Zapater, J.M., and Alonso-Blanco, C. (2012). Novel natural alleles at FLC and LVR loci account for enhanced vernalization responses in Arabidopsis thaliana. Plant, Cell & Environment **35**: 1672–1684.

Schulz, E., Tohge, T., Zuther, E., Fernie, A.R., and Hincha, D.K. (2016). Flavonoids are determinants of freezing tolerance and cold acclimation in Arabidopsis thaliana. Sci Rep **6**: 34027.

Singh, A. and Roy, S. (2017). High altitude population of Arabidopsis thaliana is more plastic and adaptive under common garden than controlled condition. BMC Ecol **17**: 39.

Smith, W.K. and Knapp, A.K. (1990). Ecophysiology of High Elevation Forests. In Plant Biology of the Basin and Range, Ecological Studies. (Springer Berlin Heidelberg: Berlin, Heidelberg), pp. 87–142.

Suter, L., Rüegg, M., Zemp, N., Hennig, L., and Widmer, A. (2014). Gene Regulatory Variation Mediates Flowering Responses to Vernalization along an Altitudinal Gradient in Arabidopsis. Plant Physiol. **166**: 1928–1942.

Suzuki, N. and Mittler, R. (2006). Reactive oxygen species and temperature stresses: A delicate balance between signaling and destruction. Physiol Plant **126**: 45–51.

Takahashi, Y., Zhang, J., Hsu, P.-K., Ceciliato, P.H.O., Zhang, L., Dubeaux, G., Munemasa, S., Ge, C., Zhao, Y., Hauser, F., and Schroeder, J.I. (2020). MAP3Kinase-dependent SnRK2-kinase activation is required for abscisic acid signal transduction and rapid osmotic stress response. Nat Commun **11**: 12.

Therneau, T. (2012). The lmekin function. Rochester, MN: Mayo Clinic.

Tripathi, A.M., Singh, A., Singh, R., Verma, A.K., and Roy, S. (2019). Modulation of miRNA expression in natural populations of A. thaliana along a wide altitudinal gradient of Indian Himalayas. Sci Rep **9**: 441.

Tusiime, F.M., Gizaw, A., Gussarova, G., Nemomissa, S., Popp, M., Masao, C.A., Wondimu, T., Abdi, A.A., Mirré, V., Muwanika, V., Eilu, G., and Brochmann, C. (2020). Afro-alpine flagships revisited: Parallel adaptation, intermountain admixture and shallow genetic structuring in the giant senecios (Dendrosenecio). PLoS ONE **15**: e0228979.

Tyagi, A., Yadav, A., Tripathi, A.M., and Roy, S. (2016). High light intensity plays a major role in emergence of population level variation in Arabidopsis thaliana along an altitudinal gradient. Sci Rep **6**: 26160.

Vasseur, F., Exposito-Alonso, M., Ayala-Garay, O.J., Wang, G., Enquist, B.J., Vile, D., Violle, C., and Weigel, D. (2018). Adaptive diversification of growth allometry in the plant *Arabidopsis thaliana*. Proc Natl Acad Sci USA **115**: 3416–3421.

Vidigal, D.S., Marques, A.C.S.S., Willems, L.A.J., Buijs, G., Méndez-Vigo, B., Hilhorst, H.W.M., Bentsink, L., Picó, F.X., and Alonso-Blanco, C. (2016). Altitudinal and climatic associations of seed dormancy and flowering traits evidence adaptation of annual life cycle timing in *Arabidopsis thaliana*: Climatic adaptation of annual life cycles. Plant, Cell & Environment **39**: 1737–1748.

Wang, H., Prentice, I.C., Davis, T.W., Keenan, T.F., Wright, I.J., and Peng, C. (2017). Photosynthetic responses to altitude: an explanation based on optimality principles. New Phytol **213**: 976–982.

Ward, J.K. and Strain, B.R. (1997). Effects of low and elevated CO2 partial pressure on growth and reproduction of Arabidopsis thaliana from different elevations. Plant Cell Environ **20**: 254–260.

Wickham, H., Chang, W., and Wickham, M.H. (2016). Package 'ggplot2.' Create elegant data visualisations using the grammar of graphics. Version **2**: 1–189.

Wise, R.R. (1995). Chilling-enhanced photooxidation: The production, action and study of reactive oxygen species produced during chilling in the light. Photosynth Res **45**: 79–97.

Wolfe, M.D. and Tonsor, S.J. (2014). Adaptation to spring heat and drought in northeastern Spanish *Arabidopsis thaliana.* New Phytol **201**: 323–334.

Yamamoto, H.Y., Nakayama, T.O.M., and Chichester, C.O. (1962). Studies on the light and dark interconversions of leaf xanthophylls. Archives of Biochemistry and Biophysics **97**: 168–173.

Zhu, Y., Siegwolf, R.T., Durka, W., and Körner, C. (2010). Phylogenetically balanced evidence for structural and carbon isotope responses in plants along elevational gradients. Oecologia **162**: 853–863.

Supplemental Methods

1. Planting and Germination Conditions in Experiments 1–3

Seeds from each line were bulked in a grow room between 15–25ºC with a 16-hour photoperiod. At 21 days after planting, plants were vernalized at 4ºC for ten weeks with an 8-hour photoperiod, then returned to initial growth conditions until maturity. At full maturity, seeds were harvested and stored in tubes at 4ºC. We then stratified seeds in distilled water at 4ºC in darkness for four days and planted four seeds per pot in randomly generated locations, in SC-10 Cone-tainersTM (1.5-inch diameter, 164 ml) in a RL98 rack within small flow trays (Stuewe and Sons, Tangent, OR, USA). Plants were grown in a Percival growth chamber (Model PGC-40L2, Percival Scientific, Inc., Perry, IA) maintaining well-watered conditions throughout the experiments. In Experiment 1 and 2 pots were filled with 50% autoclaved growing media (Premier pro-mix PGX), 25% medium commercial grade sand, and 25% calcined clay (TURFACE® ALL SPORT PRO™, Turface Athletics™, PROFILE Products LLC, Buffalo Grove, IL), with 2.5 cm of potting mix as topsoil to assist plants in germination and initial growth. In Experiment 3, proportions were 20% autoclaved growing media, 40% clay, and 40% calcined clay. Pots were covered with Glad Press'n Seal Wrap (The Glad Products Company; Oakland, CA) to prevent seed drying, and removed after germination. After the first true leaves expanded (up to 23 days after planting), pots were thinned to one healthy, representative plant per pot.

2. Harvesting for the DPPH assay in Experiments 2 and 3

Rosettes from each treatment were harvested in a randomly selected order within 2–3 days. All ecotype replicates per treatment were combined during harvest, cleaned with DI water and blotted dry. After taking fresh aboveground mass, tissue was immediately flash frozen using liquid nitrogen for 10 seconds, placed in a centrifuge tube with a 5 mm stainless steel grinding ball, and then stored at –20ºC (Experiment 2) or –80ºC (Experiment 3) for at least 48 hours. The tissue was then ground to a fine powder while remaining frozen. Acidified methanol 0.1% (v/v) was immediately added to each sample at a consistent ratio of 1 ml per 40 mg fresh tissue. Samples were repeatedly inverted and vortexed for 30 seconds and subsequently incubated at –20ºC for 48 hours, transferred to deep well plates, and centrifuged for 15 minutes at 3500 rpm at 4°C to obtain the supernatant to analyze for antioxidant activity.

One week prior to sample analyses, we prepared Trolox standards of 1000, 750, 500, 250, 100, and 0 ug/ml (Experiment 2) or of 300, 200, 100, 50, 25, and 0 ug/ml (Experiment 3). One day prior to sample analyses, 1,1-diphenyl-2-picrylhydrazyl (DPPH) solution was prepared from a stock of 36 mg of DPPH dissolved and well-mixed in 200 ml of methanol in a light-proof bottle. The DPPH solution was first checked for absorbance at 515 nm using an absorbance plate reader (BioTek Cytation 3 Imaging Reader with Gen5 version 2.04 software, Winooski, VT), if necessary, the solution was adjusted to achieve an absorbance value of 1.1 (+/- 0.1), and lights were turned off to prevent degradation. In a 375 ul flat bottom 96-well microplate (Dot Scientific, Inc., Burton MI) each well was filled with 250 ul of DPPH solution followed by 15 ul of each sample's supernatant along with the prepared Trolox standards. Each plate included at least one blank well (250 ul DPPH with 15 ul acidified methanol). Plates were incubated in darkness at room temperature for 40–60 minutes with the lid on. Following incubation, plates were run for absorbance at 515 nm and 24°C and observed values were compared to the standard curve.

3. Sequencing and Variant Calling

Total genomic DNA of the eight newly sequenced accessions (Table S1) was extracted from young leaves using the cetyltrimethylammonium bromide (CTAB) method (Murray and Thompson, 1980). At least 4 µg of genomic DNA was used to construct pair-end sequencing libraries which were sequenced on the Illumina HiSeq 2500 platform (Illumina, San Diego, USA). On average, a total of 1.22 Gb data for each accession was used for further analysis.

After trimming Illumina tags with Trimmomatic (Bolger et al., 2014), pair-end reads from each accession were mapped to the *Arabidopsis thaliana* TAIR10 genome (Araport11 assembly) using bwa (Li and Durbin, 2009) (Version: 0.7.12) with the following parameters: bwa -n 0.01 -o 2 -l 16500 -t 7. Read alignments were converted into the BAM format, sorted according to mapping coordinates, and PCR duplicates removed using the Picard (http://broadinstitute.github.io/picard/; Version: 2.8.2) and SAMtools (Li et al., 2009) programs with default parameters.

To accurately identify SNPs, the low-quality and short alignments (mapping quality score <30 and length <30 bp) were filtered and BAM files were then indexed using SAMtools. SNP detection was performed using GATK HaplotypeCaller (DePristo et al., 2011) in -ERC GVCF mode, which finds and realigns indels on the fly. Then, all genomic VCFs (gVCFs) were combined for joint genotyping with CombineGVCFs which produces a set of joint-called SNP and indels ready for filtering. To reduce the number of false positives, a high SNP confidence score was set with the following parameters: -stand_call_conf 30 -stand_emit_conf 40. We then splitted variants into SNPs and indels with SelectVariants and chose only biallelic SNPs with --restrictAllelesTo BIALLELIC. Finally, to ensure the quality of variant calling, we used the following hard filters with VariantFiltration: QUAL < 30.0, SQR > 3.0, FS > 60.0 and MQ < 40.0, to obtain a single VCF file with unphased loci for the eight eastern African accessions.

We then used VCFtools (Danecek et al., 2011) to filter a published VCF file with 1217 accessions (Durvasula et al., 2017) and obtain only biallelic SNPs in the five nuclear chromosomes. We then added the 8 newly sequenced eastern African accessions to this VCF with BCFtools. After obtaining a merged VCF file with all accessions, we used Beagle (May 2020 version release) (Browning and Browning, 2009) to phase genotypes and impute missing SNPs based on linkage disequilibrium with default parameters. We used this VCF to produce a GDS file in the SNPRelate R package (Zheng et al., 2012). With this genofile, we obtained a list of 11’500,298 polymorphic SNPs (7’878,411 and 5’624,313 for ecotypes with flowering time data from western Mediterranean and central Asia, respectively) and a SNP matrix from the ecotypes here studied (261 with sequence data, 192 with flowering time data for the western Mediterranean, and 109 for central Asia). These files were used to produce a BED file from the list of SNPs with a custom R code, and to assess Identity by State and produce an ibs matrix for all loci to account for population genetic structure in GWAS.

4. Growing conditions for focused physiological study on 11 ecotypes

After 4 days of dark stratification at 4°C in sterile water or gibberellic acid (800 PPM), we planted 2–3 seeds per ecotype in 8.89 × 8.89 cm pot (SQN0350-0-B66, Hummert International, Earth City, MO, USA) filled with soil-less potting mix (10-12050, Berger BM2 germination mix; Hummert International). To maintain moisture until germination, trays (65-69630; Hummert International) were filled with 2 cm water from the bottom and covered with a dome (15218200, Hummert International). Trays were positioned in a controlled-environment chamber (AR-66L2, Percival, Perry, IA, USA) with a 16-hour photoperiod, air temperature controlled at 18/21 °C (night/day) and 60% relative humidity. Light intensity at the leaf level was controlled at 200

μmol m^{-2} s^{-1}. After 4–5 days since germination, we thinned the seedlings to one healthy seedling per pot. Pots were watered with 150 ppm liquid fertilizer (Peter's 20-10-20 general purpose fertilizer, 25#, Peters Inc., Allentown, PA, USA) twice a week and repositioned at random locations.

Supplemental Results

1. Analysis of RGB color data

To characterize the multidimensional color variation of leaves (and their extracts) among genotypes and environments in Experiments 2 and 3, we calculated Principal Components of RGB color (Fig. S1 B and C), revealing distinct patterns between experiments. In Experiment 2, higher amounts of red + green light loaded positively on $PC1_{LeavesColor}$ while higher amounts of blue light loaded positively on $PC2_{LeavesColor}$. Thus, under high light leaves were darker (lower values of PC1) and bluer (higher values of PC2) than under lower light where leaves were light green, probably due to reduced pigments (Fig. S1 B). For leaf extracts in Experiment 3, higher amounts of blue + green light loaded positively on $PC1_{ExtractsColor}$ while red light loaded negatively on $PC2_{ExtractsColor}$. Thus, under night-time freezing extracts were less green (lower values of PC1) and dark orange to deep red (lower values of PC2), suggesting more anthocyanins and carotenoids than chlorophylls, while under no freezing extracts tended to be light green/orange, likely indicative of chlorophylls and xanthophylls (Fig. S1 C). Photographs taken on rosettes prior to harvest in both experiments showed that plants were darker/bluer under stress from high light and night-time freezing, thus extracts from leaves give greater information on pigment diversity than RGB color assessments from leaf photographs.

2. Trait variation among regions in Experiment 1

ANOVA and post hoc Tukey tests revealed that several traits varied among regions. These included flowering time at 16 ºC ($F(2,207)=6.12$, $p=0.003$), with European ecotypes having earlier flowering than central Asian and western Mediterranean (post hoc Tukey $p<0.002$). Leaf temperature ($F(2,240)=4.71$, $p=0.01$), with hotter leaves in western Mediterranean than in central Asia (post hoc Tukey $p=0.01$). Rosette diameter ($F(2,240)=6.55$, $p=0.002$), with smaller rosettes in central Asia than in Europe and western Mediterranean (post hoc Tukey $p\leq0.04$). Rosette compactness ($F(2,240)=29.82$, $p<0.0001$), with less compact rosettes in western Mediterranean than in central Asia and Europe (post hoc Tukey $p<0.0001$). $\delta^{15}N$ ($F(2,237)=5.71$, $p=0.004$), with higher $\delta^{15}N$ in central Asia than in Europe and western Mediterranean (post hoc Tukey $p\leq0.01$). Leaf C:N ($F(2,237)=15.63$, $p<0.0001$), with lower C:N in western Mediterranean, followed by central Asia, and lastly by Europe (post hoc Tukey $p\leq0.03$). Stomata length ($F(2,76)=3.05$, $p=0.05$), with shorter stomata in Europe than in central Asia (post hoc Tukey $p=0.05$).

3. Trait covariation within regions in Experiment 1

To dissect region-specific patterns of covariation among life history-physiology traits in our ecotypes, we performed pairwise correlations globally and within regions (Fig. S2–S6). We focus on significant relationships ($p<0.05$) that vary among regions. Later flowering was associated with higher $\delta^{13}C$ only in western Mediterranean ($r=0.54$) and European ecotypes ($r=0.65$). In both regions, flowering time and $\delta^{13}C$ were affected by the same traits, but these differed between regions. In western Mediterranean ecotypes, higher stomatal density correlated with higher $\delta^{13}C$ ($r=0.39$) and later flowering time ($r=0.49$). In European ecotypes, lower C:N correlated with higher $\delta^{13}C$ ($r= -0.56$) and later flowering time ($r= -0.56$).

Supplemental Figures

Figure S1. Eigenvector plot of the loadings of **A**. 9 variables onto the first and second principal components (PCs) of trait space that describe phenotypes in Experiment 1 along with flowering time data at 10 and 16 ºC in 215 ecotypes, colored by region with symbols following Fig.1. **B**–**C**. Blue, red and green lights onto the first and second PCs of color space that describe phenotypes in **B**. Experiment 2 in leaves of 108 ecotypes and **C**. Experiment 3 in leaf extracts of 151 ecotypes. For all plots, each arrow represents a vector of loadings. The direction of each arrow represents the relationship of a trait (or color) to PC1 and PC2 and the length of the vector represents the strength of that relationship. In B and C ecotypes are colored by treatment using the RGB measurements from a representative phenotype.

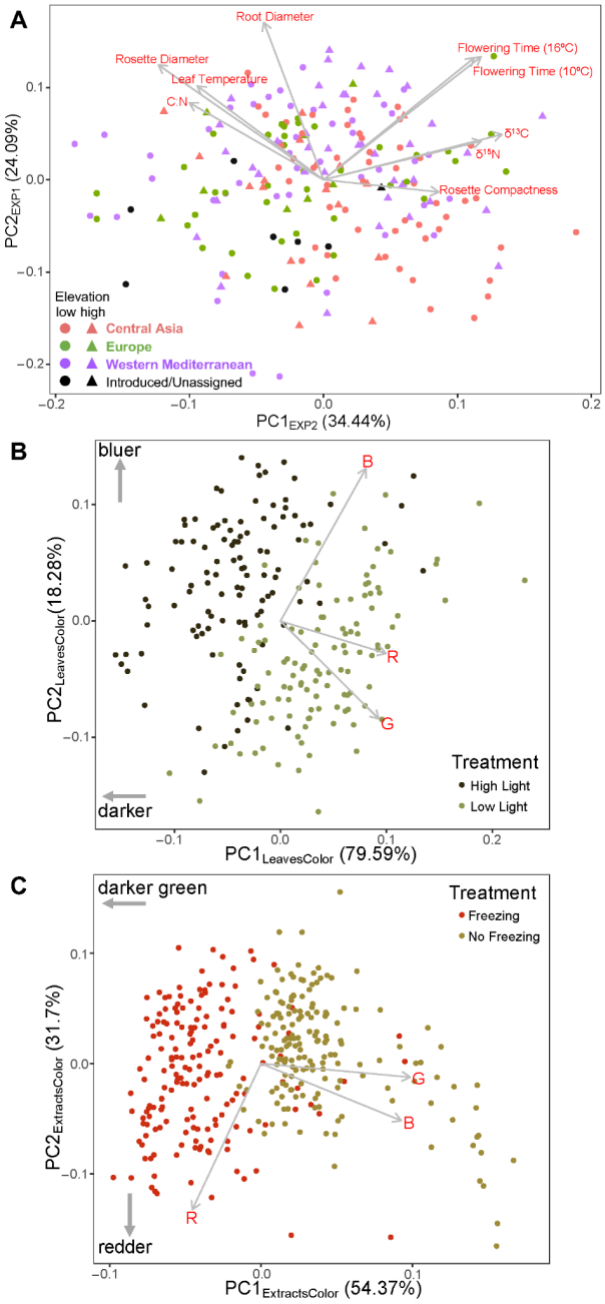

Figure S2. Pairwise correlations of traits from Experiments 1–3 and flowering time taken in all ecotypes. Circles represent significant correlations, size, and darkness their magnitude, positive correlations are blue, and negative are red.

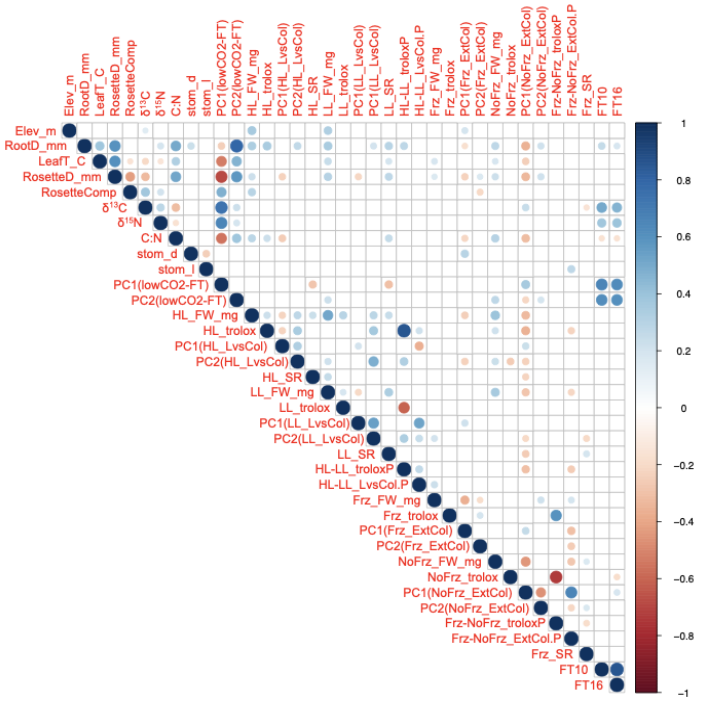

Figure S3. Pairwise correlations of traits from Experiments 1–3 and flowering time taken in central Asian ecotypes. Circles represent significant correlations, size, and darkness their magnitude, positive correlations are blue, and negative are red.

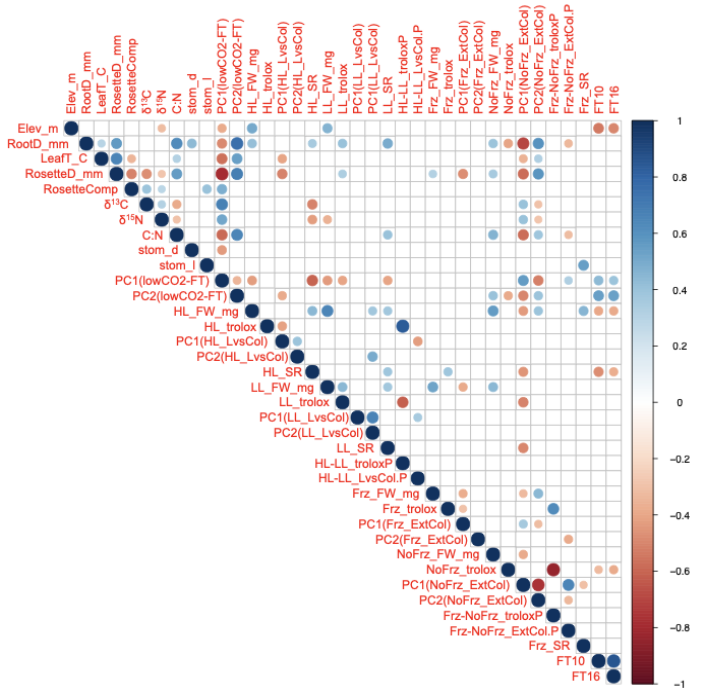

Figure S4. Pairwise correlations of traits from Experiments 1–3 and flowering time taken in European ecotypes. Circles represent significant correlations, size, and darkness their magnitude, positive correlations are blue, and negative are red.

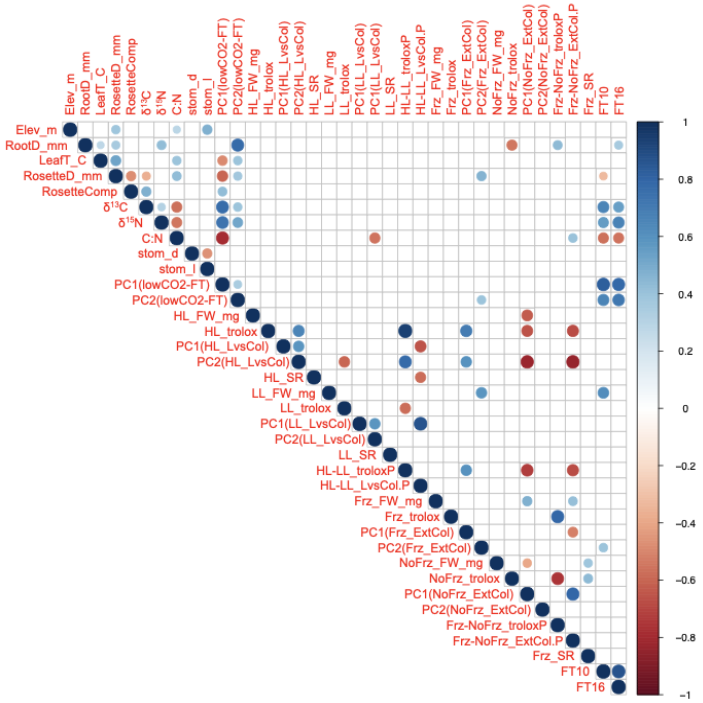

Figure S5. Pairwise correlations of traits from Experiments 1–3 and flowering time taken in western Mediterranean ecotypes. Circles represent significant correlations, size, and darkness their magnitude, positive correlations are blue, and negative are red.

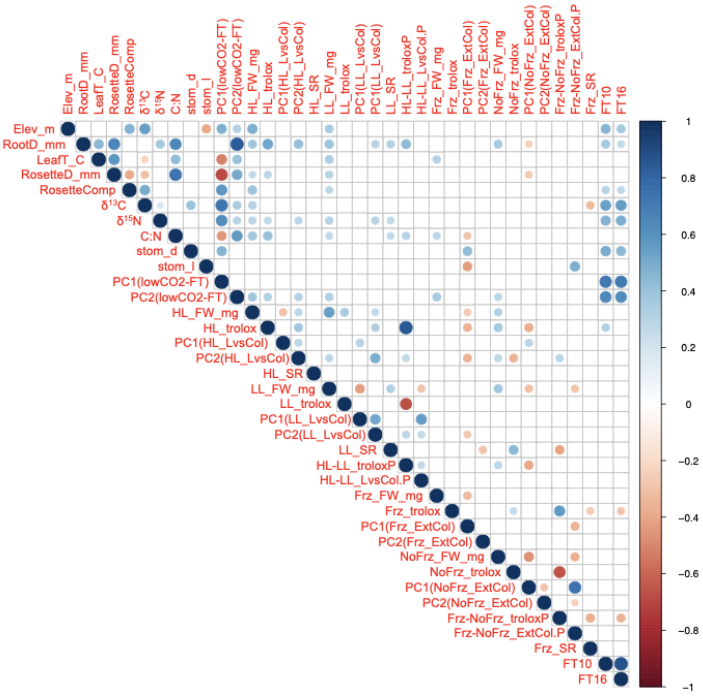

Figure S6. Pairwise correlations of traits from Experiment 3 in eastern African ecotypes. Circles represent significant correlations, size, and darkness their magnitude, positive correlations are blue, and negative are red.

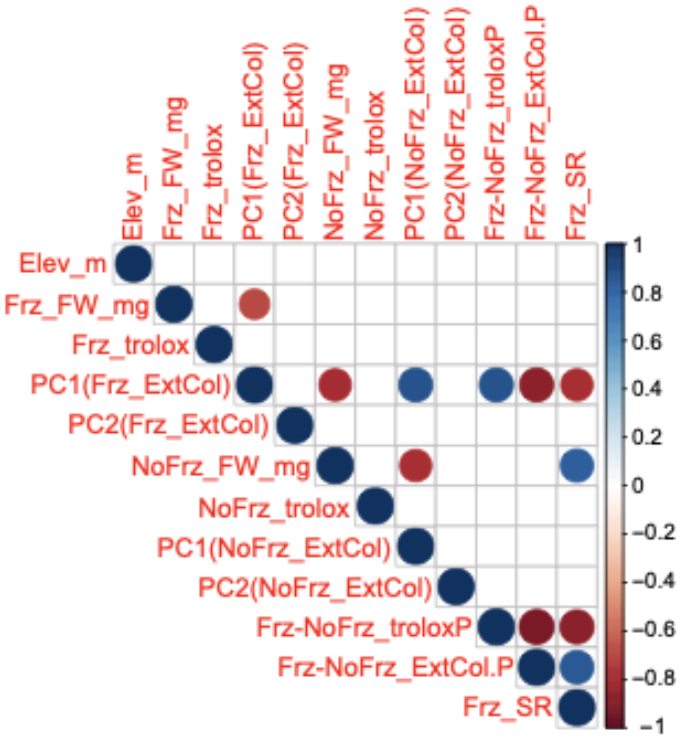

Figure S7. Representative NPQ induction and relaxation curve showing NPQ kinetics parameters. By fitting the NPQ data to exponential equations, six distinct parameters were obtained: ***residual***$_{light}$ - initial NPQ prior to light exposure; ***time constant***$_{light}$ - the rate of NPQ induction following light exposure; ***asymptote***$_{light}$ - maximum value of NPQ estimated from the asymptote; and when light was removed ***time constant***$_{dark}$ - rate of NPQ relaxation; ***asymptote***$_{dark}$ - minimum value of NPQ estimated from asymptote and ***residual***$_{dark}$ - remaining NPQ estimated from the difference between the asymptote and zero during the recovery.

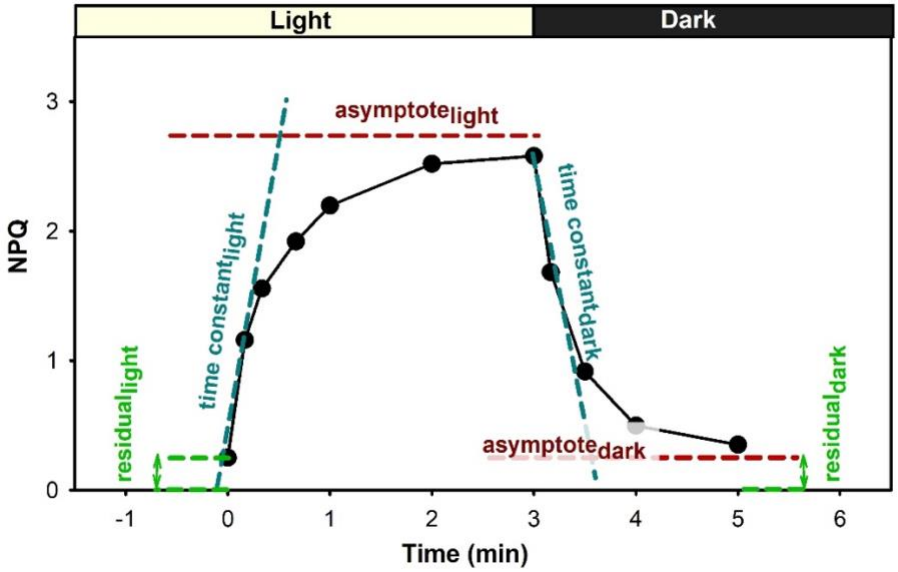

Figure S8. Effect of cold on NPQ kinetics for three subsequent light-dark cycles in 11 ecotypes. (A–C) *residual*$_{light}$ - the initial NPQ prior to light exposure; (D–F) *time constant*$_{light}$ - the rate of NPQ induction following light exposure; (G–I) *asymptote*$_{ligh}$ - maximum value of NPQ estimated from asymptote; and then when light was removed (J–L) *time constant*$_{dark}$ - the rate of NPQ relaxation (M–O) *asymptote*$_{dark}$ - minimum value of NPQ estimated from asymptote; and (P–R) *residual*$_{dark}$ - remaining NPQ (residual) estimated from the difference between the asymptote and zero during the recovery, with each estimated for three sequential light-dark cycles. Cyan bars represent cold treatment and gray bars represent control. Error bars indicate SEM (N=5–6 replicates). Different letters indicate significant differences from a post-hoc Tukey HSD test (p < 0.05). Green WM: western Mediterranean; EA: eastern Africa.

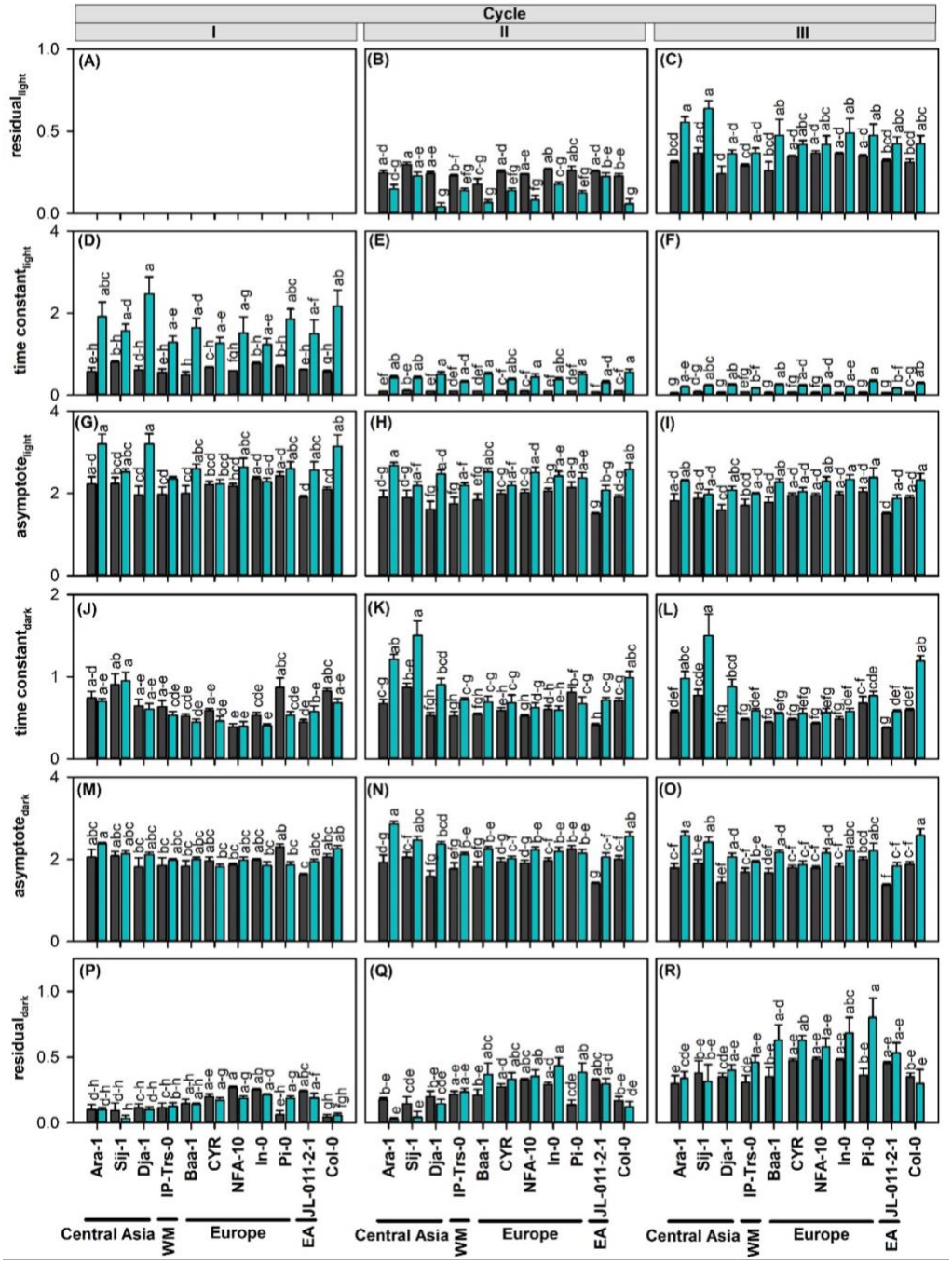

Figure S9. Effect of drought on NPQ kinetics for three subsequent light-dark cycles in 9 ecotypes. (A–C) *residual*$_{light}$ - the initial NPQ prior to light exposure; (D–F) *time constant*$_{light}$ - the rate of NPQ induction following light exposure; (G–I) *asymptote*$_{ligh}$ - maximum value of NPQ estimated from asymptote; and then when light was removed (J–L) *time constant*$_{dark}$ - the rate of NPQ relaxation (M–O) *asymptote*$_{dark}$ - minimum value of NPQ estimated from asymptote; and (P–R) *residual*$_{dark}$ - remaining NPQ (residual) estimated from the difference between the asymptote and zero during the recovery, with each estimated for three sequential light-dark cycles. Orange bars represent drought and gray bars control. Error bars indicate SEM (N=9–10 replicates, 5 in Dja-1). Different letters indicate significant differences from a post-hoc Tukey HSD test ($p < 0.05$). WM: western Mediterranean; EA: eastern African.

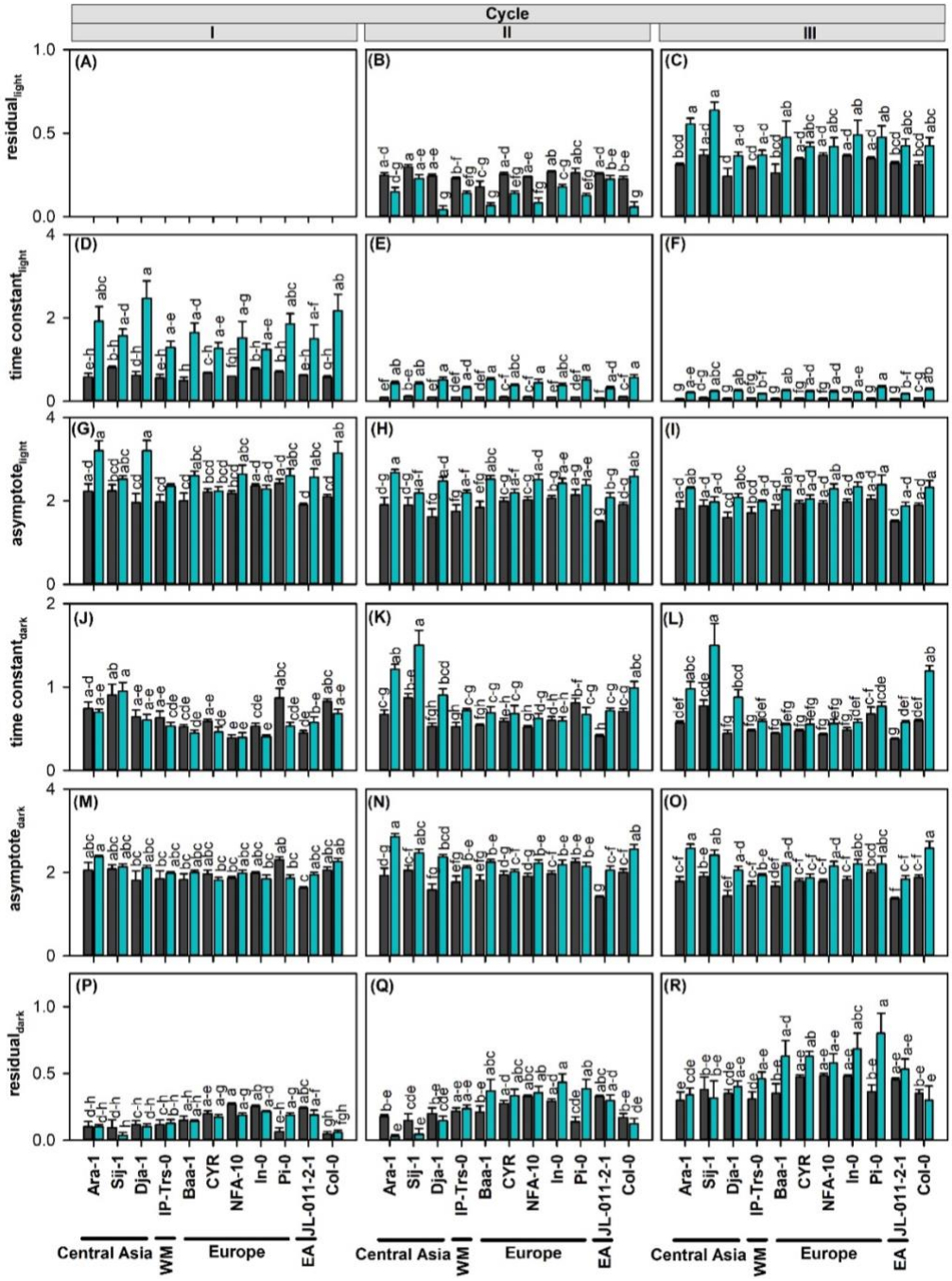

Figure S10. Aboveground biomass of 11 ecotypes grown under control conditions. (A) Representative picture of ecotypes; (B) fresh weight; (C) dry weight; (D) dry matter content (%). Error bars indicate SEM (N = 4–6 replicates). Different letters indicate significant differences from a post-hoc Tukey HSD test ($p < 0.05$). WM: western Mediterranean; EA: eastern African.

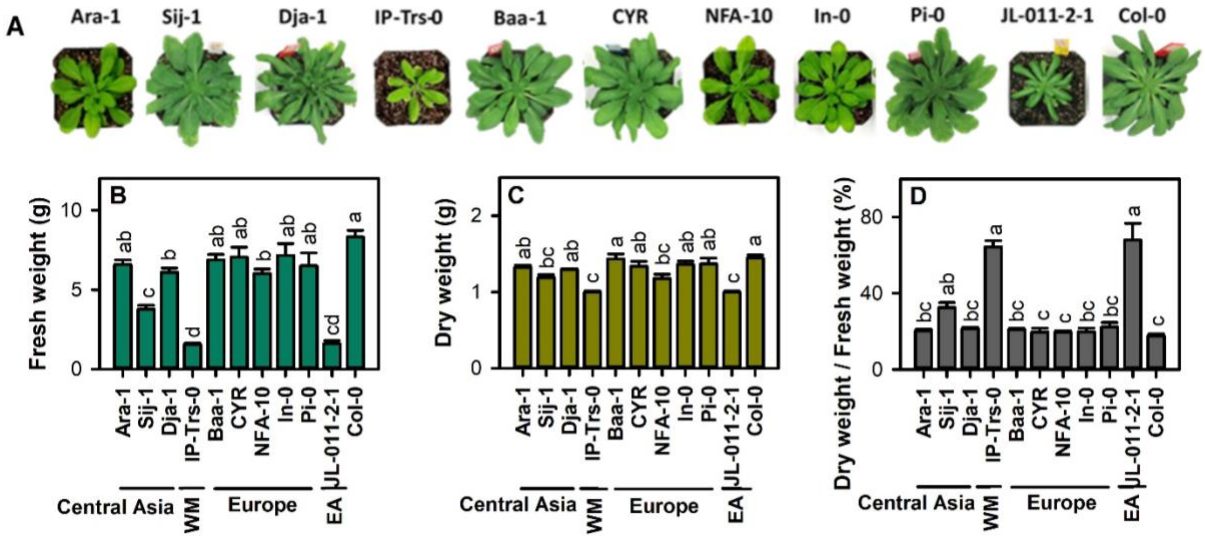

Figure S11. Linear regressions on elevation of phenotypes measured in Experiment 3. Left panels are traits measured under night-time freezing/day thaw and right panels under no night-time freezing. Ecotypes and fitted lines are colored by region (east: red, north: green, south: blue, west: purple). **A**, **B**. Fresh aboveground mass (mg). **C**, **D**. Antioxidant activity (mg/mg). **E**, **F**. PC1 of leaf color. **G**, **H**. PC2 of leaf color. **I**. Plasticity in antioxidant activity (mg/mg). **J**. Survival rate under night freeze/day thaw (most stressful treatment). No linear relationships were significant.

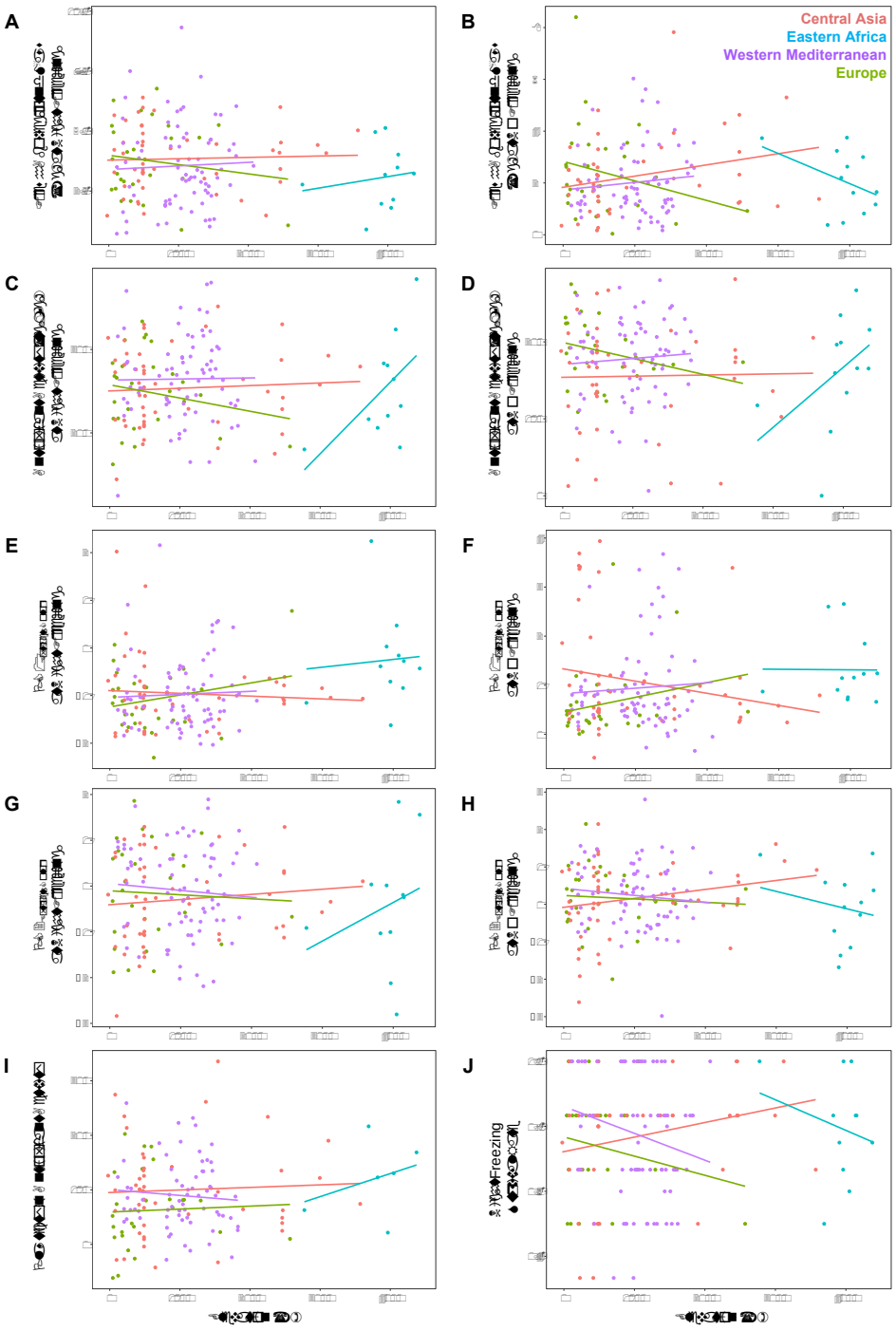

Figure S12. *DOG1* haplotype variation relative to elevation (left) and flowering time (right) in ecotypes from **A**, **B**. the western Mediterranean, **C**, **D**. Europe, and **E**, **F**. central Asia

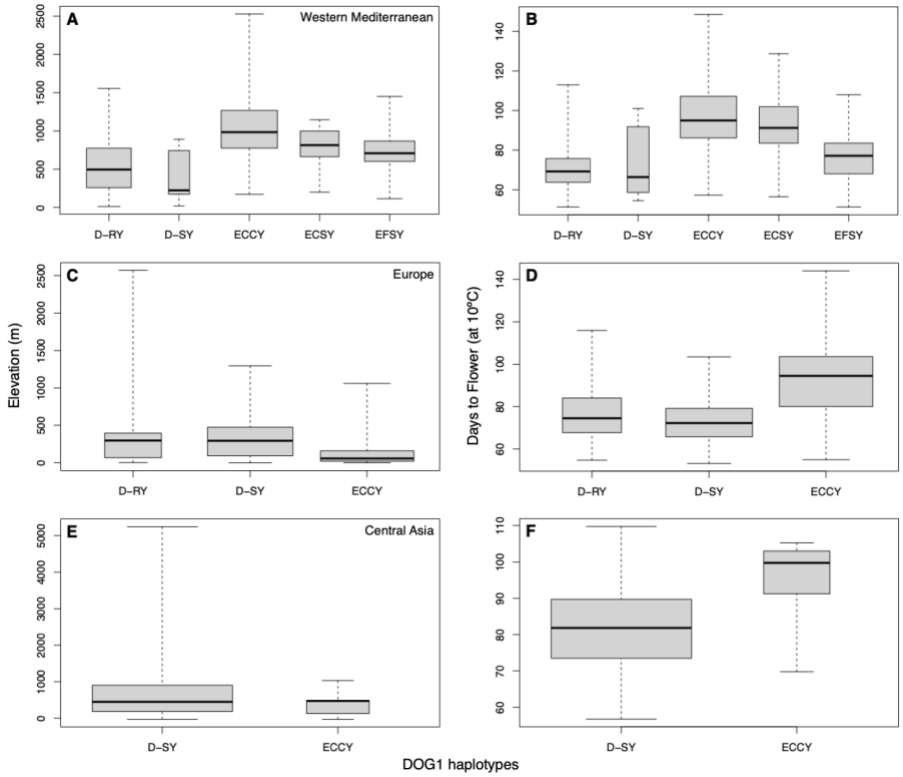

Supplemental Tables (most are Microsoft Excel files)
Table S1. Ecotypes used in all experiments
Table S2. List of environmental variables used in the PCA of Fig. 1
Table S3. Percival programs and HOBO data for Experiment 1
Table S4. Percival programs and HOBO data for Experiment 2
Table S5. Percival programs and HOBO data for Experiment 3
Table S6. ANOVA on NPQ kinetics in response to cold
Table S7. ANOVA on NPQ kinetics in response to drought
Table S8. Photosynthesis parameters in response to steady-state and dynamic light changes
Table S9. Quantification of photosynthesis related traits in a focused physiological panel
Table S10. Linear regressions of traits on elevation and selected environmental variables
Table S11. FDR values of linear models
Table S12. Linear mixed-effects models of traits on elevation while accounting for kinship
Table S13. ANOVA and Tukey HSD comparing traits and climatic variables among regions
Table S14. Top SNPs and functional gene annotation in Flowering Time GWAS
Table S15. Top SNPs and functional gene annotation for GWAS in Experiment 1
Table S16. Top SNPs and functional gene annotation for GWAS in Experiment 2
Table S17. Top SNPs and functional gene annotation for GWAS in Experiment 3
Table S18. Variation of selected SNPs on elevation
Table S19. F_{ST} values for SNPs in chr 4, comparing Moroccan ecotypes to everything else

Table S6. Results of ANOVA for an effect of ecotype (E), cold treatment (T) and interaction E × T on 17 parameters of NPQ kinetics obtained by fitting an exponential equation to curves of NPQ induction (light) and relaxation (dark) in three subsequent light-dark cycles. Bolded *p*-values indicate a significant effect.

Parameter	*p*-value		
	Ecotype (E)	Cold treatment (T)	E × T
Light-dark Cycle I			
time constant$_{light}$	**0.02**	**<0.0001**	**0.03**
asymptote$_{light}$	**0.01**	**<0.0001**	**0.001**
time constant$_{dark}$	**<0.0001**	**0.007**	0.08
asymptote$_{dark}$	**<0.0001**	0.1	**0.003**
residual$_{dark}$	**<0.0001**	0.3	**0.04**
Light-dark Cycle II			
residual$_{light}$	**<0.0001**	**<0.0001**	0.08
time constant$_{light}$	**0.0003**	**<0.0001**	**0.04**
asymptote$_{light}$	**0.0003**	**<0.0001**	0.05
time constant$_{dark}$	**<0.0001**	**<0.0001**	**<0.0001**
asymptote$_{dark}$	**<0.0001**	**<0.0001**	**<0.0001**
residual$_{dark}$	**<0.0001**	0.1	**0.0002**
Light-dark Cycle III			
residual$_{light}$	**0.002**	**<0.0001**	0.2
time constant$_{light}$	**0.006**	**<0.0001**	**0.01**
asymptote$_{light}$	**<0.0001**	**<0.0001**	0.6
time constant$_{dark}$	**<0.0001**	**<0.0001**	**0.0002**
asymptote$_{dark}$	**<0.0001**	**<0.0001**	**0.02**
residual$_{dark}$	**<0.0001**	**<0.0001**	0.07

Table S7. Results of ANOVA for an effect of ecotype (E), drought treatment (T) and interaction E × T for 17 parameters of NPQ kinetics obtained by fitting an exponential equation to curves of NPQ induction (light) and relaxation (dark) in three subsequent light-dark cycles. Bolded *p*-values indicate a significant effect.

Parameter	*p*-value		
	Ecotype (E)	Drought treatment (T)	E × T
Light-dark Cycle I			
time constant$_{light}$	**<0.0001**	**0.04**	**<0.0001**
asymptote$_{light}$	**<0.0001**	**<0.0001**	**0.002**
time constant$_{dark}$	**<0.0001**	**0.002**	**<0.0001**
asymptote$_{dark}$	**<0.0001**	**<0.0001**	**<0.0001**
residual$_{dark}$	**<0.0001**	0.6	**<0.0001**
Light-dark Cycle II			
residual$_{light}$	**<0.0001**	**<0.0001**	**0.01**
time constant$_{light}$	**<0.0001**	**0.008**	**<0.0001**
asymptote$_{light}$	**<0.0001**	**<0.0001**	**0.0009**
time constant$_{dark}$	**<0.0001**	**<0.0001**	**<0.0001**
asymptote$_{dark}$	**<0.0001**	**<0.0001**	**<0.0001**
residual$_{dark}$	**<0.0001**	**0.05**	**<0.0001**
Light-dark Cycle III			
residual$_{light}$	**<0.0001**	**<0.0001**	**0.0006**
time constant$_{light}$	**<0.0001**	**<0.0001**	**<0.0001**
asymptote$_{light}$	**<0.0001**	**<0.0001**	**0.0001**
time constant$_{dark}$	**<0.0001**	**0.05**	**<0.0001**
asymptote$_{dark}$	**<0.0001**	**<0.0001**	**0.006**
residual$_{dark}$	**<0.0001**	**<0.0001**	**0.002**

Table S8. Characteristics of the steady state and dynamic response of leaf fluorescence and gas exchange to light intensity (Q) in eight ecotypes (with elevation of origin in parenthesis). Numbers represent means and SEM are indicted in brackets (N = 3–6 biological replicates). The p-values indicate effect of the ecotype. Different letters indicate significant differences from a post-hoc Tukey HSD test ($p < 0.05$).

	Ecotype								***p*-value**
	Central Asia		**Europe**		**eastern Africa**		**USA**		
	Sij-1 (2459 m)	**Dja-1** (2995 m)	**Baa-1** (22 m)	**CYR** (52 m)	**In-0** (1576 m)	**Pi-0** (2570 m)	**JL-11** (4078 m)	**Col-0** (NA)	
Steady-state A_n, C_i, g_s, $_i$WUE, J and NPQ as a function of light intensity									
A_{n50}	1.50^{b} (0.11)	1.82^{ab} (0.17)	1.88^{ab} (0.14)	2.07^{a} (0.13)	1.98^{ab} (0.04)	1.64^{ab} (0.08)	1.74^{ab} (0.13)	1.96^{ab} (0.05)	**0.009**
A_{n500}	13.95^{a} (0.54)	8.98^{b} (1.36)	13.69^{a} (0.54)	11.27^{ab} (0.45)	11.83^{ab} (0.30)	10.10^{ab} (0.74)	9.69^{b} (1.30)	11.26^{ab} (0.88)	**0.002**
A_{n1000}	15.51^{a} (0.50)	10.13^{c} (1.55)	14.82^{ab} (0.46)	12.11^{abc} (0.49)	12.86^{abc} (0.32)	11.13^{bc} (0.75)	10.81^{bc} (1.43)	12.34^{abc} (0.96)	**0.0008**
C_{i50}	367.1^{a} (10.0)	350.0^{ab} (10.0)	344.6^{b} (2.7)	360.2^{ab} (5.5)	357.3^{ab} (3.6)	356.9^{ab} (6.8)	361.8^{ab} (3.2)	357.0^{ab} (6.1)	**0.03**
C_{i500}	311.8 (4.0)	271.3 (13.2)	295.4 (5.2)	292.2 (7.4)	297.5 (2.6)	303.6 (9.5)	310.3 (3.9)	294.3 (10.7)	0.09
C_{i1000}	316.1 (2.8)	285.3 (14.4)	303.9 (5.7)	297.8 (7.6)	305.1 (2.6)	312.3 (6.9)	316.5 (6.1)	303.2 (8.4)	0.1
g_{s50}	0.151 (0.031)	0.074 (0.012)	0.064 (0.004)	0.114 (0.012)	0.094 (0.011)	0.086 (0.013)	0.095 (0.009)	0.109 (0.024)	0.06
g_{s500}	0.291^{a} (0.025)	0.124^{b} (0.025)	0.234^{ab} (0.017)	0.190^{ab} (0.016)	0.205^{ab} (0.009)	0.194^{ab} (0.022)	0.197^{ab} (0.035)	0.206^{ab} (0.036)	**0.03**
g_{s1000}	0.344 (0.025)	0.163 (0.040)	0.281 (0.017)	0.217 (0.022)	0.243 (0.011)	0.239 (0.033)	0.250 (0.052)	0.245 (0.039)	0.06
$_i$WUE$_{50}$	15.59 (6.29)	26.32 (6.27)	29.72 (1.73)	19.86 (3.45)	21.69 (2.27)	22.03 (4.29)	18.94 (2.02)	21.85 (3.86)	0.1
$_i$WUE$_{500}$	48.69 (2.57)	74.99 (8.38)	59.11 (3.33)	61.41 (4.71)	57.98 (1.67)	54.44 (5.97)	50.29 (2.56)	60.12 (6.83)	0.09
$_i$WUE$_{1000}$	45.75 (1.79)	65.96 (9.21)	53.57 (3.62)	57.81 (4.83)	53.03 (1.64)	48.80 (4.31)	46.20 (3.95)	54.37 (5.41)	0.1
J_{50}	15.76^{abc} (0.07)	15.90^{abc} (0.04)	16.04^{ab} (0.08)	16.00^{abc} (0.07)	16.15^{a} (0.12)	15.55^{bc} (0.12)	15.46^{c} (0.19)	15.50^{bc} (0.13)	**0.0005**
J_{500}	99.39^{a} (2.01)	79.15^{b} (7.75)	97.81^{ab} (2.29)	80.48^{ab} (3.53)	84.66^{ab} (2.63)	83.44^{ab} (4.95)	82.66^{ab} (3.94)	81.34^{ab} (3.96)	**0.006**
J_{1000}	103.81^{a} (3.23)	79.49^{b} (8.97)	96.28^{ab} (3.54)	81.82^{b} (3.93)	83.58^{ab} (2.46)	86.14^{ab} (5.45)	85.81^{ab} (3.63)	81.35^{b} (4.31)	**0.004**
NPQ$_{50}$	0.110^{c} (0.01)	0.173^{a} (0.002)	0.142^{abc} (0.004)	0.140^{abc} (0.01)	0.130^{bc} (0.01)	0.137^{abc} (0.008)	0.141^{abc} (0.006)	0.155^{ab} (0.007)	**0.001**
NPQ$_{500}$	0.95^{b} (0.06)	1.44^{a} (0.20)	1.07^{ab} (0.06)	1.29^{ab} (0.08)	1.36^{ab} (0.03)	1.14^{ab} (0.14)	1.19^{ab} (0.07)	1.32^{ab} (0.08)	**0.04**
NPQ$_{1000}$	1.72^{b} (0.04)	2.10^{a} (0.07)	1.92^{ab} (0.06)	1.96^{ab} (0.03)	2.15^{a} (0.04)	1.9^{ab} (0.10)	1.88^{ab} (0.06)	2.00^{ab} (0.04)	**0.002**
$\Phi_{PSIImax}$	0.309 (0.002)	0.311 (0.003)	0.315 (0.001)	0.316 (0.001)	0.313 (0.002)	0.308 (0.003)	0.310 (0.003)	0.306 (0.002)	0.05
J_{max}	109.7^{a} (3.7)	82.4^{b} (9.4)	100.0^{ab} (3.8)	83.9^{b} (3.8)	86.2^{b} (2.5)	88.6^{ab} (6.0)	88.1^{ab} (4.0)	84.2^{b} (4.7)	**0.002**
Φ_{CO2max}	0.065^{a} (0.001)	0.060^{ab} (0.004)	0.056^{ab} (0.001)	0.063^{a} (0.001)	0.063^{ab} (0.003)	0.053^{ab} (0.004)	0.049^{b} (0.005)	0.061^{ab} (0.002)	**0.008**
A_{sat}	18.3^{a} (0.5)	11.7^{c} (1.7)	16.6^{ab} (0.4)	13.7^{bc} (0.6)	14.5^{abc} (0.6)	12.7^{bc} (1.0)	12.0^{c} (1.6)	13.8^{abc} (1.1)	**0.0003**
R_d	-1.52^{b} (0.15)	-0.81^{a} (0.07)	-0.91^{ab} (0.10)	-0.90^{ab} (0.15)	-1.00^{ab} (0.17)	-0.78^{a} (0.17)	-0.58^{a} (0.09)	-0.91^{ab} (0.08)	**0.001**

A_n, C_i, g_s, $_i$WUE, Φ_{PSII}, J and NPQ as a function of light intensity under fluctuating light									
A_{n50}	1.33 (0.11)	1.71 (0.24)	1.79 (0.11)	1.66 (0.24)	1.77 (0.10)	1.40 (0.13)	1.48 (0.14)	1.64 (0.09)	0.3
A_{n500}	14.18^{a} (0.46)	10.85^{a} (1.50)	13.72^{a} (0.43)	12.29^{a} (0.25)	12.27^{a} (0.27)	10.64^{a} (0.87)	10.48^{a} (1.33)	12.14^{a} (0.78)	**0.01**
C_{i50}	382.7^{a} (0.8)	375.3^{b} (1.7)	368.1^{b} (5.0)	375.7^{b} (1.4)	372.1^{b} (3.6)	380.0^{ab} (1.7)	378.9^{ab} (1.6)	377.5^{ab} (5.1)	**0.005**
C_{i500}	320.3 (3.4)	292.9 (11.4)	297.1 (12.6)	307.9 (7.8)	308.7 (3.8)	317.0 (3.0)	321.9 (7.8)	314.6 (9.2)	0.2
g_{s50}	0.231 (0.019)	0.162 (0.014)	0.139 (0.026)	0.181 (0.027)	0.153 (0.022)	0.190 (0.018)	0.189 (0.030)	0.242 (0.038)	0.1
g_{s500}	0.333 (0.026)	0.186 (0.044)	0.252 (0.030)	0.249 (0.027)	0.242 (0.013)	0.230 (0.012)	0.263 (0.055)	0.281 (0.040)	0.2
$_i$WUE$_{50}$	5.84^{b} (0.48)	10.50^{a} (1.00)	15.00^{a} (3.17)	9.21^{ab} (0.86)	12.50^{a} (2.22)	7.64^{ab} (1.06)	8.27^{ab} (1.01)	9.13^{ab} (3.18)	**0.003**
$_i$WUE$_{500}$	43.33 (2.17)	61.13 (7.33)	58.08 (7.95)	51.46 (4.96)	50.99 (2.40)	45.98 (1.78)	42.95 (4.95)	47.23 (5.90)	0.2
J_{50}	14.84 (0.08)	14.73 (0.17)	15.11 (0.14)	14.83 (0.12)	15.13 (0.13)	14.44 (0.26)	14.37 (0.26)	14.6 (0.18)	0.06
J_{500}	96.41 (2.14)	85.02 (6.90)	94.92 (3.00)	85.91 (2.89)	85.99 (2.40)	88.67 (4.83)	86.00 (3.18)	84.5 (3.45)	0.1
NPQ$_{50}$	0.434 (0.021)	0.496 (0.020)	0.458 (0.018)	0.515 (0.031)	0.450 (0.025)	0.490 (0.039)	0.469 (0.063)	0.569 (0.037)	0.2
NPQ$_{500}$	1.19^{a} (0.04)	1.50^{a} (0.17)	1.29^{a} (0.07)	1.42^{a} (0.08)	1.56^{a} (0.05)	1.27^{a} (0.14)	1.31^{a} (0.06)	1.58^{a} (0.08)	**0.02**
$\Phi_{PSIImax}$	0.287^{a} (0.002)	0.280^{a} (0.005)	0.294^{a} (0.003)	0.286^{a} (0.004)	0.293^{a} (0.003)	0.277^{a} (0.006)	0.278^{a} (0.005)	0.280^{a} (0.004)	**0.04**
J_{max}	110.0^{a} (4.1)	85.3^{b} (8.4)	100.7^{ab} (4.1)	86.5^{b} (3.9)	88.3^{b} (2.6)	89.4^{ab} (5.7)	90.8^{ab} (3.4)	86.5^{b} (4.3)	**0.004**
Φ_{CO2max}	0.059^{a} (0.002)	0.045^{a} (0.002)	0.054^{a} (0.001)	0.054^{a} (0.003)	0.054^{a} (0.003)	0.045^{a} (0.004)	0.043^{a} (0.006)	0.053^{a} (0.003)	**0.01**
A_{sat}	18.3^{a} (0.5)	11.3^{c} (1.7)	16.5^{ab} (0.5)	14.0^{abc} (0.7)	14.3^{abc} (0.5)	12.4^{bc} (0.9)	12.1^{bc} (1.7)	13.9^{abc} (1.1)	**0.0004**
R_d	-1.53^{b} (0.19)	-0.40^{a} (0.18)	-0.85^{ab} (0.07)	-0.97^{ab} (0.29)	-0.88^{ab} (0.19)	-0.69^{ab} (0.21)	-0.70^{ab} (0.27)	-0.90^{ab} (0.18)	**0.04**

A_{n50}, A_{n500} and A_{n1000} – net CO_2 assimilation at light intensities 50, 500 and 1000 µmol m^{-2} s^{-1}, respectively (µmol m^{-2} s^{-1}); **A_{sat}** - light-saturated rate of net assimilation rate; an asymptote of A/Q curve (µmol m^{-2} s^{-1}); **C_{i50}, C_{i500}** and **C_{i1000}** - intercellular CO_2 concertation at light intensities 50, 500 and 1000 m^{-2} s^{-1}, respectively (µmol mol^{-1}); **g_{s50}, g_{s500}** and **g_{s1000}** – stomatal conductance at light intensities 50, 500 1000 µmol m^{-2} s^{-1}, respectively (mol H_2O m^{-2} s^{-1}); **iWUE$_{50}$**, **iWUE$_{500}$** and **iWUE$_{1000}$** - intrinsic water-use efficiency at light intensities 50, 500 and 1000 µmol m^{-2} s^{-1} calculated as A_{n50} / g_{s50}, A_{n500}/ g_{s500}, and A_{n1000}/ g_{s1000}, respectively (µmol CO_2 mol^{-1} H_2O); **J_{50}, J_{500}, J_{1000}** - linear electron transport rate at light intensity of 50, 500 and 1000 µmol m^{-2} s^{-1}, respectively (µmol m^{-2} s^{-1}); **J_{max}** – maximal linear electron transport rate calculated as asymptote of *J*/*Q* curve (µmol m^{-2} s^{-1}); **NPQ$_{50}$, NPQ$_{500}$** – non-photochemical quenching at light intensity of 50 and 500 µmol m^{-2} s^{-1}, respectively (unit less); **R_d** - mitochondrial respiration rate in the light estimated from intercept of the *A*/*Q* response (µmol m^{-2} s^{-1}); **ΦCO_{2max}** – maximum quantum efficiency of leaf net CO_2 assimilation estimated from initial slope of *A*/*Q* curve (CO_2 / photon); **$\Phi PSII_{max}$** – maximum quantum efficiency of linear electron transport estimated from the initial linear part of the *J*/*Q* curves (e^- / photon).

Table S9. Quantification of photosynthesis related pigments. Numbers represent means and SEM are indicated in brackets (*N* = 4–6 biological replicates). The *p*-values indicate the effect of the ecotype. Different letters indicate significant differences from a post-hoc Tukey HSD test ($p \leq 0.05$).

	Ecotype								***p*-value**
	Central Asia		**Europe**		**eastern Africa**		**USA**		
	Sij-1 (2459 m)	**Dja-1** (2995 m)	**Baa-1** (22 m)	**CYR** (52 m)	**In-0** (1576 m)	**Pi-0** (2570 m)	**JL-11** (4078 m)	**Col-0** (NA)	
Chl *a* ($g\ m^{-2}$)	0.250^{a} (0.014)	0.217^{ab} (0.005)	0.230^{ab} (0.008)	0.199^{bc} (0.004)	0.209^{bc} (0.009)	0.229^{ab} (0.007)	0.128^{c} (0.003)	0.229^{ab} (0.010)	0.0007
Chl *b* ($g\ m^{-2}$)	0.124^{a} (0.007)	0.108^{ab} (0.009)	0.108^{ab} (0.004)	0.088^{bc} (0.004)	0.098^{abc} (0.011)	0.110^{ab} (0.002)	0.067^{c} (0.001)	0.103^{abc} (0.003)	0.0009
Chl *a* + *b*	0.374^{a} (0.021)	0.325^{ab} (0.013)	0.338^{ab} (0.010)	0.287^{bc} (0.006)	0.307^{bc} (0.019)	0.339^{ab} (0.008)	0.195^{c} (0.004)	0.333^{bc} (0.012)	0.0007
Chl *a* / *b*	2.03 (0.05)	2.06 (0.16)	2.14 (0.07)	2.28 (0.10)	2.19 (0.19)	2.08 (0.04)	1.92 (0.02)	2.22 (0.08)	0.05
Total Car ($g\ m^{-2}$)	0.0532^{a} (0.0014)	0.0353^{cd} (0.0012)	0.0412^{bc} (0.0015)	0.0347^{d} (0.0011)	0.0350^{cd} (0.0007)	0.0398b cd (0.0012)	0.0202^{e} (0.0006)	0.0423^{b} (0.0022)	<0.0001
Chl *a* + *b* / Total Car	7.04^{c} (0.40)	9.26^{ab} (0.56)	8.22^{abc} (0.26)	8.32^{cb} (0.29)	8.76^{ab} (0.45)	8.52^{abc} (0.14)	9.65^{a} (0.17)	7.91^{bc} (0.22)	0.002

Car - total carotenoids; chl *a* - chlorophyll *a*; chl *b* – chlorophyll *b*.

Supplemental References

Bolger, A.M., Lohse, M., and Usadel, B. (2014). Trimmomatic: a flexible trimmer for Illumina sequence data. Bioinformatics **30**: 2114–2120.

Browning, B.L. and Browning, S.R. (2009). A unified approach to genotype imputation and haplotype-phase inference for large data sets of trios and unrelated individuals. The American Journal of Human Genetics **84**: 210–223.

Danecek, P. et al. (2011). The variant call format and VCFtools. Bioinformatics **27**: 2156–2158.

DePristo, M.A., Banks, E., Poplin, R., Garimella, K.V., Maguire, J.R., Hartl, C., Philippakis, A.A., Del Angel, G., Rivas, M.A., and Hanna, M. (2011). A framework for variation discovery and genotyping using next-generation DNA sequencing data. Nature genetics **43**: 491–498.

Li, H. and Durbin, R. (2009). Fast and accurate short read alignment with Burrows–Wheeler transform. bioinformatics **25**: 1754–1760.

Li, H., Handsaker, B., Wysoker, A., Fennell, T., Ruan, J., Homer, N., Marth, G., Abecasis, G., and Durbin, R. (2009). The sequence alignment/map format and SAMtools. Bioinformatics **25**: 2078–2079.

Murray, M.G. and Thompson, W.F. (1980). Rapid isolation of high molecular weight plant DNA. Nucleic Acids Research **8**: 4321–4326.

Zheng, X., Levine, D., Shen, J., Gogarten, S.M., Laurie, C., and Weir, B.S. (2012). A high-performance computing toolset for relatedness and principal component analysis of SNP data. Bioinformatics **28**: 3326–3328.